ISSN : 0019-5693

INDIAN JOURNAL
OF
THEORETICAL PHYSICS

VOLUME 70 **NOS. 3, 4**

JULY, 2022 – DECEMBER, 2022

Published by the
CALCUTTA INSTITUTE OF THEORETICAL PHYSICS
(Formerly, INSTITUTE OF THEORETICAL PHYSICS)
"BIGNAN KUTIR"
4/1, MOHAN BAGAN LANE, KOLKATA-700004

(Peer-reviewed Journal)

ISSN : 0019-5693

INDIAN JOURNAL
OF
THEORETICAL PHYSICS

[Founder President : Late Prof. K. C. Kar, D. Sc.]

VOLUME 70 NOS. 3, 4

JULY, 2022 –DECEMBER, 2022

INDIAN JOURNAL
OF
THEORETICAL PHYSICS

"BIGNAN KUTIR"
4/1, MOHAN BAGAN LANE, KOLKATA-70004, INDIA

SUBSCRIPTION RATE

INDIA : For Library (Institute)

₹1500.00 for each volume

FOREIGN : $ 350 for each volume

Drafts, Orders, Enquiries & Claim for Non-Receipt of Journal should be sent to :

CALCUTTA INSTITUTE OF THEORETICAL PHYSICS
(Formerly, INSTITUTE OF THEORETICAL PHYSICS)
"BIGNAN KUTIR"
4/1, MOHAN BAGAN LANE, KOLKATA-700004, India

C O N T E N T S

1. The Kinetic Energy Spectrum for Turbulence in a Stably Stratified Fluid : Kolmogorov or The Elusive Bolgiano-Obukhoy?

– *Jayanta K Bhattacharjee* 85

2. On MHD Blood Flow Through Permeable Bifurcated Arteries in Tumor Treatments.

– *Anup Kumar Karak and Ruma Bagchi* 113

3. A Brief Review on Metallic Nanoparticles

– *Subhendu Chandra* 129

4. One Day Seminar by CITP in Collaboration with Physics Department of RKM Residential College, Narendrapur, Kolkata 149

INDIAN JOURNAL OF THEORETICAL PHYSICS, VOL 70, NOS. 3 & 4, 2022

The Kinetic Energy Spectrum for Turbulence in a Stably Stratified Fluid : Kolmogorov or The Elusive Bolgiano-Obukhov?

Jayanta K Bhattacharjee

School of Physical Sciences,

Indian Association for the Cultivation of Science,

Jadavpur, Kolkata 700032,

India

[Abstract : In a homogeneous isotropic fluid the kinetic energy spectrum is supposed to follow the Kolmogorov law. This fact has been very clearly established both experimentally and numerically. More than sixty years ago it was predicted independently by Bolgiano and by Obukhov that for a stratified fluid (like our atmosphere which supports a temperature gradient), the kinetic energy spectrum should be different. The degree of stratification is determined by the Richardson number Ri which is a ratio of the "stratification potential energy" to the kinetic energy. It would be "natural" to find the Bolgiano-Obukhov spectrum at a relatively high Richardson number. However, till now this spectrum has never been clearly seen.

In this article we introduce and discuss the energy spectrum for fully developed turbulence and try to provide the reason behind the inability to capture the Bolgiano-Obukhov spectrum. We use an analysis based on an almost forgotten Heisenberg- Chandrasekhar picture of turbulence to establish the crossover function for Kolmogorov to Bolgiano-Obukhov scaling in fully developed

turbulence in a stably stratified fluid. We find that there are actually two crossovers-one from the Kolmogorov to the Bolgiano-Obukhov form and the other from the Bolgiano-Obukhov to a pre-dissipative form. For a given Richardson number, the former happens at a wave-number proportional to $Ri^{-3/4}$ and the latter at a wave-number proportional to $Ri^{-3/16}$. This severely restricts the range over which a pure Bolgiano-Obukhov scaling can be seen and explains the elusive nature of that scaling law].

1. Introduction to Turbulent Flows

One of the striking results in the theory of fully developed turbulence in a homogeneous fluid is the scaling law for the energy spectrum $E(k)$ at a given wave-number k in the inertial range. The energy spectrum is related to the total kinetic energy K as

$$K = \frac{1}{2V}\int \left\langle u^2 \right\rangle d^3r = \frac{1}{2}\int \left\langle u_j(k)u_j(-k)\right\rangle \frac{d^3k}{(2\pi)^3} = \int_0^\infty E(k)dk \quad \ldots (1.1)$$

In the above $u_j(\vec{r},t)$ is the random turbulent velocity field, $u_j(k)$ its Fourier transform, the angular bracket denotes an appropriate ensemble average and V is the total volume of the fluid. The inertial range is the range of spatial scales where the wave-number k (inverse of the spatial scale) is smaller than wave-numbers in the dissipation range (where viscous forces dominate) and larger than those corresponding to the large length scales where energy is injected in the fluid to maintain a non-equilibrium steady state. The scales are easily visualized from the stirring of a cup of tea to mix the sugar. We stir the liquid at a scale which is characterized by the radius of the cup (a few centimetres). This energy is dissipated by the viscosity of the liquid which operates at a

sub-micron scale. The ratio of the scales is about five orders of magnitude. This is where Kolmogorov[1] argued that the energy spectrum has the universal form $E(k) \propto k^{-5/3}$.

To get a feel for the logic behind the Kolmogorov result , we write down the primary equation for three dimensional incompressible fluid flow with velocity $u_i (i = 1,2,3)$ [incompressibility implies $\partial_i u_i = 0$ (divergence free flow)]

$$\dot{u}_i + u_j \partial_j u_i = -\partial_i p + \nu \nabla^2 u_i + f_i \qquad \ldots \ (1.2)$$

In the above equation, the pressure is denoted by 'p' (it is actually the pressure per unit density i.e. the constant density of the incompressible fluid has been absorbed in the pressure), $\vec{f}$ is an external force and ν is the kinematic viscosity. To find the rate of change of the total kinetic energy of the fluid, we need to consider the quantity $\int d^3 r \dot{u}_j u_j$ and use Eq.(1.2) to substitute for $\dot{u}_j$.

We will get four terms. The equality $\int dV u_j \partial_j p = \int dV \partial_j (u_j p)$ holds since the velocity field is divergence free and using Gauss's law this integral becomes the surface integral of the vector $p\vec{u}$ with the surface as far away as we want. In particular the surface can be chosen where the fluid velocity vanishes (there is no source) and hence the integral is zero. Similarly for the term $u_i (u_j \partial_j u_i)$, we can write it as $\partial_j (u_j u^2 / 2)$ and the logic of the previous sentence makes the integral of this term zero as well. The integral $\int u_j \nabla^2 u_j dV$ can be written as the

integral of the negative of $\left(\partial_j u_i\right)^2$ and is the energy loss due to the viscous action. On the other hand, $\int dV(u_j f_j)$ is the rate of energy supply by the external force [the stirring action for the example of the coffee cup] . If these two effects are equal in magnitude then the total kinetic energy of the fluid is maintained and we have a non-equilibrium steady state of maintained turbulence. The supply of energy is at large length scales and the dissipation is at the smallest scales. The energy which is introduced at a constant rate ε is pictured to cascade down the scales without loss to be dissipated by viscous action at smallest scales.

Kolmogorov argued that if one is not too close to the dissipation scale and also significantly away from the energy input scale, then the energy spectrum $E(k)$ of turbulence is determined by only the wave-number 'k' and the strength ε of the cascading energy. The dimension of $E(k)$ is L^3/T^2 and that of ε is L^2/T^3. Since $E(k)$ is determined by ε and k, we write $E(k) = C\varepsilon^m k^n$ (the self-similar nature of the turbulent flow made famous by the Leonardo da Vinci drawing), where C is a dimension-free universal constant and the exponents need to be found by a dimensional analysis. We see that $L^3/T^2 = L^{2m-n}/T^{3m}$, leading to $m = 2/3$ and $n = -5/3$. Hence $E(k) = C\varepsilon^{2/3}k^{-5/3}$, the so-called Kolmogorov spectrum. This is one of the best known results in all of turbulence and generally known as Kolmogorov's 5/3 law.

We now shift our attention to the stably stratified fluid where the density decreases with height. The stratified fluid was first studied by Bolgiano[2] and Obukhov[3], who argued that one is supposed to encounter

an energy spectrum $E(k)$ which scales as $k^{-11/5}$ in this case. We will work with a positive temperature gradient in the z-direction which makes the stratification stable. The constant positive temperature gradient is $\Delta T / d$ with the bounding surfaces as the x-y planes located at $z = 0$ and $z = d$. The steady state temperature profile is linear in z. We work in the Boussinesque approximation[4] where the buoyancy induced temperature fluctuation around the steady state shows up only in the linear order in the velocity dynamics. We denote the dimensionless temperature fluctuation by $\theta = \delta T / \Delta T$. We also include a random forcing term $\vec{f}(\vec{r},t)$ in the velocity dynamics to inject energy at large length scales. With the buoyancy force included, the velocity dynamics (Navier-Stokes equation) becomes

$$\partial_t u_i + \left(u_j \partial_j\right) u_i = -\frac{\partial_i p}{\rho_0} - \alpha \Delta T g \theta \hat{z} + \nu \nabla^2 u_i + f_i \quad \ldots \quad (1.2)$$

The pressure field is denoted by $p(\vec{r},t)$, ρ_0 is a mean density (will be absorbed in the pressure subsequently) , α is the expansion coefficient and ν the kinematic viscosity. The dynamics of θ for stable stratification (including an external random fluctuation $h(\vec{r},t)$ at large length scales) is

$$\partial_t \theta + u_j \partial_j \theta = \lambda \nabla^2 \theta + \frac{u_z}{d} + h(\vec{r},t) \quad \ldots (1.3)$$

The dynamics of the total kinetic energy *K* follows from Eq. (1.2) as

$$V \partial_t K = \alpha \Delta T g \int \theta u_z d^3 r - \nu \int \left(\partial_i u_j\right)^2 d^3 r + \int f_j u_j d^3 r \quad \ldots (1.4)$$

The first term on the right hand side ensures that K is not conserved in the unforced, inviscid limit. In a similar vein, from Eq. (1.3) we have

$$\partial_t \frac{1}{V}\int \frac{1}{2}\theta^2 d^3r = \frac{1}{V}[\frac{1}{d}\int \theta u_z d^3r - \lambda\int (\nabla\theta)^2 d^3r + \int \theta h d^3r] \quad \ldots (1.5)$$

Between Eqns. (1.4) and (1.5), we have a conserved quantity E in the unforced and dissipation regime which is like a sum of kinetic and potential energies[5], since

$$\partial_t E = \partial_t (K + \alpha\Delta T g d \frac{1}{V}\int \frac{1}{2}\theta^2 d^3r)$$

$$= -\frac{1}{V}[\nu\int (\partial_i u_j)^2 d^3r + \lambda\alpha\Delta T g d\int (\nabla\theta)^2 d^3r - \int (f_j u_j + \theta h) d^3r] \quad \ldots (1.6)$$

The first two terms on the right hand side cause dissipation at very short length scales and the third and fourth terms inject energy at large length scales. In the unforced and inviscid limit ($\nu=\lambda=f=h=0$) the quantity $E = K + (\alpha\Delta T g d)U$ where $U = \frac{1}{2V}\int \theta^2 d^3r$ is conserved and from the structure of Eq (1.6), this quantity E is produced at large length scales (small wave-number scales) and flows down to short length scales (large wave-numbers) where it is dissipated. To compare K and U on the same footing it is best to make them have the same dimension and this is done by defining $\bar{U} = u_0^2 U$ where u_0^2 is a mean square velocity. The conserved quantity in the inviscid, unforced limit is now $K + \frac{\alpha\Delta T g d}{u_0^2}\bar{U} = K + Ri\bar{U}$ where the dimensionless number

$Ri = \frac{\alpha \Delta T g d}{u_0^2}$ is called the Richardson number. For the stably stratified fluid, this is the energy that is conserved in the absence of dissipation and external forcing. However, the energy spectrum of turbulence that one talks about is always the kinetic energy spectrum. For the energy flux, however, it is the total energy and that can lead to a very different story for the scaling laws[6,7]. It should be noted that for the convective situation (top-heavy) dealt with in Refs[8-16], the terms which are quadratic in the θ-field in Eq.(1.6) appear with a negative sign. This makes definite statements about the sign of the energy flux difficult as the flux may depend on the value of the Prandtl number. A detailed discussion can be found in Verma et al[17].

When the Richardson number becomes high, the $\bar{U}$ term can dominate the "energy" transfer and the energy spectrum will be changed because the transfer will now be engineered by the θ^2 term. The rate of transfer ε_θ will have the dimension of θ^2/t where t is time. Once again, it is important to appreciate what happens at large Richardson numbers. The scale to scale transfer of the energy E is now dominated by the dynamics of the temperature fluctuation $\theta(\mathbf{r},t)$. Apparently θ is "dimensionless" but this is not the dimension one is talking about. The dimension is the scaling dimension and corresponds to the dimension that one gets if Eq. (1.3) is going to be invariant under a scale transformation. This implies that the constant rate ε_θ at which the energy is transferred in the inertial range will have the dimension L^2/T^5. The energy spectrum $E(k)$ in this limit will be determined by ε_θ and k and is easily seen to be

$$E(k) = K_1 \varepsilon_\theta^{2/5} k^{-11/5} \quad \ldots (1.7)$$

where K_1 is a numerical constant. The above spectrum is known as the Bolgiano-Obukhov scaling law[23]. Unlike the Kolmogorov spectrum, this spectrum has hardly ever been observed. Two important exceptions are the investigations of Kumar et al[6] and Rosenberg et al[7]. Even in these two studies, the 11/5 spectrum is seen over only one decade at the most.

The scaling that we describe in Eq. (1.7) is isotropic while the situation that we have described is quite clearly anisotropic. Many of the references[18-23] do observe an anisotropic spectrum. This is why this issue was studied from a scaling perspective in Refs[24-25] and it was found that the isotropic Bolgiano-Obukhov spectrum would be a reasonable approximation when the Richardson number is of $O(1)$ and the vertical length scale is of $O(u_0^3 / \varepsilon)$ which is in agreement with the finding of Rosenberg et al[7]. In this moderately anisotropic situation, Eq.(1.7) has to be understood as an angle averaged result[26].

In a recent work[27], we suggested, based on a preliminary examination of the local energy transfer associated with Eq.(1.6), that the Bolgiano –Obukhov scaling should be seen at wave-numbers higher than those at which the Kolmogorov scaling is seen. This is anti-'common-sensical' since for large k, we will have $k^{-5/3} > k^{-11/5}$ and hence Kolmogorov spectrum should dominate. However, the 'common-sensical' result has never been seen. In fact, an examination of the data presented by Rosenberg et al[7] was actually seen to be consistent with the violation of naive reasoning. In fact, for convective turbulence a similar qualitative behaviour in co-ordinate space was seen by Kunnen et al[15].

Our next goal is to discuss the intricacies associated with the scaling of the energy spectrum $E(k)$ for the stably stratified fluid. The major issues (which have prevented a clear cut observation of the Bolgiano-Obukhov spectrum) are:

(A) The crossover from Kolmogorov spectrum to Bolgiano-Obukhov spectrum is determined by the combination $kRi^{3/4}$ with the Kolmogorov region corresponding to $kRi^{3/4} << 1$ and the Bolgiano-Obukhov region corresponding to $kRi^{3/4} > 1$. This means that even if one is at a reasonably high Richardson number, one could be seeing a Kolmogorov spectrum if the condition $kRi^{3/4} > 1$ is not satisfied. What is very likely, even if it is , one will be caught in a crossover region where the exponent will seem to lie between 1.67 and 2.2. The crossover region is consequently vital and we will obtain an exact differential equation describing the course of it.

(B) The problem gets further complicated by the fact that the Bolgiano-Obukhov spectrum crosses over to an intermediate scaling in the pre-dissipative regime. This crossover happens if $kRi^{3/16} > 1$ and hence if the Richardson number is not ideally chosen, a clear run of the exponent 2.2 would hardly be seen. We will provide an exact form for this crossover as well. Between these two crossovers , it becomes non-trivial to see a pure Bolgiano-Obukhov spectrum and this could be the reason that , unlike the Kolmogorov spectrum, there are very few instances of finding a pure Bolgiano-Obukhov spectrum.

In Sec II, we extend the previous works of Chandrasekhar[28] and Heisenberg[29,30] to study the crossover from the Kolmogorov to a

dissipative regime. We show how the Heisenberg formulation works for the moderately high Richardson number case (energy transfer by the thermal fluctuations only) and obtain a closed-form expression for the spectrum describing the transition from a Bolgiani-Obukhov form to a pre-dissipative form. In Sec III we generalize this approach to obtain a gradual crossover from the Kolmogorov spectrum to the Bolgiano-Obukhov one. We conclude with a brief summary in Sec IV.

2 Bolgiano-Obukhov to dissipation range crossover

In this section we extend the Heisenberg –Chandrasekhar[28-30] formulation to the large Richardson number situation where the energy dynamics of Eq. (1.7) contains a significant contribution from thermal fluctuations and the dynamics is primarily the dynamics of the θ-field as given by Eq.(1.3). In Fourier space the θ-dynamics is given by

$$\dot{\theta}(p) = -i\sqrt{V}\int p_j u_j(\vec{p}-\vec{q})\theta(q)\frac{d^3q}{(2\pi)^3} - \lambda p^2\theta(p) + \frac{u_3}{d} \qquad \ldots (2.1)$$

The total energy E must include the "potential energy" term in Eq. (1.12) and in Fourier space is written as

$$E = K + u_0^2 Ri\int \frac{d^3p}{2(2\pi)^3}\left\langle\theta(p)\theta^*(p)\right\rangle \qquad \ldots (2.2)$$

Dropping all constant pre-factors, we write this as $E = K + Ri\int d^3p F(p)$, where $F(p) = \left\langle\theta(p)\theta^*(p)\right\rangle$ and is the amount of "potential" energy at the scale p. It should be noted that the last term on the right hand side of Eq.(2.1) is like the first term with the momentum $p \sim d^{-1} << 1$ and hence has been ignored. In the large Richardson number situation it is the time derivative of E at a given scale

which is dominated by $\dot{F}(p)$. The energy spectrum that one talks about is, however, always the kinetic energy spectrum unless specifically mentioned otherwise.

The dynamics of the potential energy is the primary contributor to the energy flux at moderate Richardson numbers. The dynamics of $F(p)$ is (cancelling the ubiquitous Ri in this limit)

$$\dot{F}(p) = -\mathrm{Im}\sqrt{V}\theta^*(p)\int p_j u_j(p-q)\theta(q)\frac{d^3q}{(2\pi)^3} - 2\lambda p^2 F(p) \quad \ldots (2.3)$$
$$= T_\theta(p) - 2\lambda p^2 F(p)$$

In the above the first term is the transfer due to the interacting triad, $\boldsymbol{p}, \boldsymbol{q}, \boldsymbol{p}-\boldsymbol{q}$. Once again the total energy $\bar{E}(k)$ contained between the scales p=0 and p=k is obtained as $\int_0^k 4\pi p^2 F(p)dp$ and the time derivative of $\bar{E}(k)$ is the rate at which energy is leaving the region $p<k$ for the region $p>k$ and hence is the rate of energy transfer from wave-numbers below k to those above it. Hence the transfer rate, dominated by the second term in Eq.(2.2), is found as (the constant velocity scale u_0^2 is absorbed in Ri)

$$\varepsilon_\theta(k) = Ri[\int_0^k 4\pi T_\theta(p)p^2 dp - \lambda\int_0^k 4\pi p^4 F(p)dp] \quad \ldots (2.4)$$

We first take the dissipative term in the above equation and express it in terms of the energy spectrum $E(p)$ and p. The dimension of $F(p)$ is found from the dimension of $\theta(p)$. As explained before the dimension that we are talking about is the scaling dimension (how do

equations remain invariant under a scale transformation) and hence the scaling dimension of $\theta(r)$ is L/T^2 . Consequently, $F(p)$ has a scaling dimension of L^5/T^4. As a result in the second term on the right hand side of Eq. (2.4), the quantity $p^4F(p)$ has the dimension L/T^4. Expressed in terms of p and $E(p)$ it behaves as $E^2(p)p^5$. The second term on the right hand side of Eq. (2.4) now becomes (dropping numerical factors) $\int_0^k E^2(p)p^5dp$. Our task now is to cast the first term in a similar form i.e. we want to write it as $-2\lambda_{eff}\int_0^k E^2(p)p^5dp$. Once again as in the kinetic energy case, the λ_{eff} operates at all scales that are greater than k and is better written as $\int_k^\infty \bar{\lambda}_{eff}(p)dp$. As in the Kolmogorov case[28] expressing $\lambda_{\text{eff}}(p)$ (this is done simply by a dimensional analysis) in terms of $E(p)$ and p, we get (the sign has been made positive with the understanding that the flow is from low to high values of k)

$$\varepsilon_\theta(k) = Ri\left[\int_k^\infty \sqrt{\frac{E(p)}{p}}\frac{dp}{p} + \lambda\right]\int_0^k E^2(p)p^5dp \qquad \ldots (2.5)$$

With $\varepsilon_\theta(k)$ set equal to a constant ε we obtain the crossover from the inertial range scaling to a pre-dissipative scaling for Bolgiano-Obukhov turbulence.

Taking a derivative of Eq. (2.5) with respect to k when $\varepsilon_\theta(k)$ is a constant, gives

$$\left[\int_k^\infty \sqrt{\frac{E(p)}{p^{3/2}}}dp + \lambda\right] E^2(k)k^5 = \sqrt{\frac{E(k)}{k^3}}\int_0^k E^2(p)p^5 dp \qquad \ldots (2.6)$$

Defining $y(k) = \int_0^k E^2(p)p^5 dp$, we can write Eq. (2.6) as

$$\lambda + \int_k^\infty \sqrt{\frac{E(p)}{p^{3/2}}}dp = \frac{1}{k^2(k^3E(k))^{3/2}}\, y(k) \qquad \ldots (2.7)$$

Further, defining $\sqrt{E(p)p^{3/2}}$ as $g^{1/4}$, the above equation becomes

$$\lambda + \int_k^\infty \frac{g(p)^{1/4}}{p^3}dp - \frac{y(k)}{k^2 g(k)^{3/4}} = 0 \qquad \ldots (2.8)$$

The definition of $y(k)$ shows $\frac{dy}{dk} = k^5E^2(k) = \frac{g(k)}{k}$ and using this in Eq. (2.8) to change the variable *p* to *y*, we arrive at

$$\lambda + \int_{y(k)}^\infty \frac{dy}{k^2 g^{3/4}} - \frac{1}{k^2}\frac{y(k)}{g^{3/4}} = 0 \qquad \ldots (2.9)$$

Differentiating the above equation with respect to *y* yields (note that

$$\frac{d(k^2)}{dy} = \frac{2k^2}{g(k)} - \frac{1}{g^{3/4}} + \frac{2y}{g^{7/4}} - \frac{d}{dy}\left(\frac{y}{g^{3/4}}\right) = 0 \qquad \ldots (2.10)$$

leading to the differential equation $\frac{dg}{dy} - \frac{8g}{3y} = -\frac{8}{3}$ with the solution $g(y) = \frac{8y}{5} - Ay^{8/3}$ where A is a constant. The relation $\frac{dy}{dk} = \frac{g}{k}$ allows us to write

$$\ln k = \int \frac{dy}{g(y)} + \text{const.} \qquad \ldots (2.11)$$

Integrating we find

$$y = \frac{\beta k^{8/5}}{(1+\alpha k^{8/3})^{3/5}} \qquad \ldots (2.12)$$

where α and β are constants. We use the definition of $y(k)$ to write

$$E^2(k)k^5 = \frac{dy}{dk} = \frac{8\beta}{5}\frac{k^{3/5}}{\left(1+\alpha k^{8/3}\right)^{8/5}} \qquad \ldots (2.13)$$

In the low k inertial range, the k term in the denominator is unimportant and we get

$$E(k) \propto k^{-11/5} \qquad (2.14)$$

-the desired Bolgiano spectrum. For high values of k the crossover is to a $E(k) \propto k^{-13/3}$ form, which is less steep than the Kolmogorov to viscous crossover.

We now need to discuss the Richardson number dependence of the coefficients α and β in Eq.(2.13) above. For this, we need to go back to Eq.(1.7) and note that $E(k) \propto \varepsilon_\theta{}^{2/5}$ and using Eq. (2.4), we get $E(k) \propto Ri^{2/5}$. Using Eq.(2.13) in the inertial range we get $\beta \propto Ri^{4/5}$. In the high k range, dissipation plays a more important role and hence the spectrum there will be determined by the dissipation coefficient λ and not Ri. In the high wave-number range the spectrum will be independent of Ri if $\alpha \propto \sqrt{Ri}$. This implies that the spectrum will be proportional to

$k^{-13/3}$ for wave-numbers $k >> Ri^{-3/16}$. This is our first result, and it states that to see the Bolgiano- Obukhov spectrum, we need to focus on wave-numbers which satisfy $kRi^{3/16} < 1$. We define a crossover wave-number $k_C = Ri^{-3/16}$. For $k < k_C$, one has the Bolgiano –Obukhov spectrum and for $k > k_C$, one enters the dissipation range with a $k^{-13/3}$ spectrum. Since the coefficient α in Eq.(2.13) is proportional to $\sqrt{Ri}$, we can write Eq.(2.13) as

$$E(k) = \bar{E}\frac{(k/k_C)^{-11/5}}{\left[1+\left(\frac{k}{k_C}\right)^{8/3}\right]^{4/5}} \qquad \ldots (2.15)$$

The above formula clearly shows the transition from the Bolgano-Obukhov spectrum to a dissipation influenced spectrum as the wave-number increases past the crossover wave-number k_C. In the next section, we present the Kolmogorov to Bolgiano-Obukhov spectrum which will yield another constraint on the range where one can see the stratified fluid spectrum. It should be clear that our calculation does not fix the coefficient of the Ri involving terms. So the exact range where the desired spectrum will be seen is not being set down but a clear idea of where to look for it and the high probability of being in a crossover range forever are the two points that we want to bring out.

3. The Kolmogorov to Bolgiano-Obukhov crossover

In this section we use the technique developed above to obtain the crossover from the Kolmogorov to the Bolgiano-Obukhov spectrum. A preliminary version of this can be found in Ref [27]. We begin by noting

that the time derivative of the $E(k)$ obtained from the full energy expression in the first line of Eq. (1.5) gives an energy flux which is simply the sum of the kinetic energy flux and the "potential energy" flux of the previous section with the latter weighted by the appropriate factor of $\alpha\Delta Tgd$. In this section we will focus on the inertial range crossover only and hence drop the dissipative terms. The total energy flux $\varepsilon_T(k)$ across the wave-number k is given by the appropriate combination of $\dot{C}(p)$ and $\dot{F}(p)$ where $C(p)=\langle u_\alpha(p)u_\alpha(-p)\rangle$ is the velocity correlation function. In analogy with the previous section the rate of total energy transfer from wave-numbers below 'k' to wave-numbers above 'k' is

$$\varepsilon_T(k)=\int_0^k 4\pi p^2\left[\dot{C}(p)+Ri\dot{F}(p)\right] \qquad \ldots (3.1)$$

Since we are in the inertial range the dissipative terms will be dropped and we have the energy transfer rate given by

$$\varepsilon_T(k)=\int_k^\infty \frac{dp}{p}\sqrt{\frac{E(p)}{p}}\left[\int_0^k p^2E(p)dp+Ri\int_0^k p^5E^2(p)dp\right] \qquad \ldots (3.2)$$

The first term on the right hand side of the above equation is exactly the term used by Heisenberg [31]. We need to point out that being in the inertial range puts a limit on the wave number. The smallest allowed wave number is determined by the inverse of the system size. The largest requires that $\sqrt{E(k)/k}$ be significantly larger than ν or λ, whichever is larger. This requires $\varepsilon^{1/3}k^{-4/3}>>\nu,\lambda$ as well as $Ri^{1/5}k^{-8/5}>>\nu,\lambda$. It should be pointed out that we have absorbed a

constant dimensional factor of square of a typical velocity scale in the problem in the Richardson number written above. We define

$$y(k) = \int_0^k p^2 E(p)dp + Ri\int_0^k p^5 E(p)dp \quad \ldots (3.3)$$

$$g(k) = k^3 E(k) + Rik^6 E^2(k) \quad \ldots (3.4)$$

$$\frac{dy}{dk} = \frac{g(k)}{k} \quad \ldots (3.5)$$

Invoking the Kolmogorov picture of the inertial range where $\varepsilon_T(k)$ is a constant and taking a derivative of Eq. (3.2) with respect to *k*, we obtain (it should be noted that since the arguments leading to Eq. (3.2) from Eq.(3.1) are based on dimensional analysis, there can be unknown functions of the dimensionless variable Ri associated with the second term in Eq. (3.4) which can only be fixed by some additional constraint)

$$y(k)\sqrt{\frac{E(k)}{k^3}} = \frac{dy}{dk}\int_k^\infty \sqrt{\frac{E(p)}{p}}\frac{dp}{p} \quad \ldots (3.6)$$

Using Eq.(3.3) to express dy/dk, we get

$$\int_k^\infty \sqrt{\frac{E(p)}{p}}\frac{dp}{p} = \sqrt{\frac{E(k)}{k^3}}\frac{y(k)}{k^2E(k) + Rik^5E^2(k)}$$
$$= \frac{y(k)}{k^2}\frac{1}{\left(k^3E(k)\right)^{1/2}}\frac{1}{1 + Rik^3E(k)} \quad \ldots (3.7)$$

Solving the quadratic equation for $k^3E(k)$ in Eq. (3.4), one has

$$E(k)k^3 = \frac{2g(k)}{\left[1+4Rig(k)\right]^{1/2}+1} \quad \ldots (3.8)$$

Substituting this result in Eq. (3.7) allows us to write the left hand side of the equation as

$$\int_k^\infty \sqrt{\frac{E(p)}{p^3}}dp = \int_k^\infty \frac{dp}{p^3}\left[\frac{\sqrt{1+4Rig(p)}-1}{2Ri}\right]^{1/2}$$

$$= \int_{y(k)}^\infty \frac{dy}{p^2\sqrt{g(p)}}\left[\frac{2}{1+\sqrt{1+4Rig(p)}}\right] \quad \ldots (3.9)$$

We have used Eq. (3.5) to obtain the final form above.

Using Eq.(3.8) in the right hand side of Eq.(3.7) and noting that

$$\frac{1}{\sqrt{k^3E(k)}}\frac{1}{1+Rik^3E(k)} = \frac{y(k)}{k^2\sqrt{g(k)}}\left[\frac{2}{1+\sqrt{1+4Rig(k)}}\right]^{1/2} \quad \ldots (3.10)$$

We finally write Eq.(3.7) in the form

$$\int_{y(k)}^\infty \frac{dy}{g(p)p^2}\left[\sqrt{1+4Rig(p)}-1\right]^{1/2} = \frac{y(k)}{k^2g(k)}\left[\sqrt{1+4Rig(k)}-1\right]^{1/2} \quad \ldots (3.14)$$

Differentiating both sides of Eq (3.11) with respect to *y*, we have

$$\frac{\left(\sqrt{1+4gRi}-1\right)^{1/2}}{g(k)} = \frac{2y(k)}{g^2}\left(\sqrt{1+4Rig}-1\right)^{1/2}$$

$$-\frac{d}{dy}\left(\frac{y\left[\sqrt{1+4Rig}-1\right]^{1/2}}{g}\right) \quad \ldots (3.12)$$

Defining,

$$f(y)=\frac{\left(\sqrt{1+4Rig(k)}-1\right)^{1/2}}{g(k)} \qquad \ldots (3.13)$$

leads to

$$f=\frac{2y(k)f}{g(k)}-\frac{d}{dy}(yf) \qquad \ldots (3.14)$$

Consequently,

$$d(\ln fy^2)=2\frac{dy}{g} \qquad \ldots (3.15)$$

with the integral $\sqrt{f}\,\frac{y}{k}=C$ (constant) leading to

$$\frac{\left[\sqrt{1+4Rig(k)}-1\right]^{1/4}}{\sqrt{g(k)}}\frac{y}{k}=C \qquad \ldots (3.16)$$

From Eq (3.5), we now have the $g(k)$ given by (setting $C=\sqrt{2}Ri^{1/4}$)

$$\int_0^k \frac{g(p)}{p}dp=kg^{1/4}(k)\left[\sqrt{1+4Rig(k)}+1\right]^{1/4} \qquad \ldots (3.17)$$

A derivative takes us to the exact differential equation satisfied by $g(k)$. We find

$$\frac{dg}{dk}=\frac{4g^{7/4}(k)}{k^2}\frac{\left[1+\sqrt{1+4Rig(k)}\right]^{3/4}}{1+\frac{1+6Rig(k)}{\sqrt{1+4Rig(k)}}}-\frac{4g(k)}{k}\frac{\left[1+\sqrt{1+4Rig(k)}\right]}{1+\frac{1+6Rig(k)}{\sqrt{1+4Rig(k)}}}$$

$\ldots (3.18)$

To obtain the asymptotic answers, we need to study the limits $Ri \rightarrow 0$ (Kolmogorov) and $Ri \rightarrow \infty$ (Bolgiano-Obukhov). In the first case we obtain

$$\frac{dg}{dk} + \frac{4g}{k} = \frac{4g^{7/4}}{k^2} \quad \ldots (3.19)$$

Simply by inspection we can write down the solution as $g(k) \propto k^{4/3}$. From Eq.(3.4) we now get $E(k) \propto k^{-5/3}$ which is the Kolmogorov spectrum. For $Rig(k) >> 1$ on the other hand

$$\left[\frac{dg}{dk} + \frac{8g}{3k}\right] = \frac{2\sqrt{2}}{k^2}\frac{g(k)^{13/8}}{Ri^{1/8}} \quad \ldots (3.20)$$

In this limit inspection yields $g(k) \propto k^{8/5}$ and this in conjunction with Eq.(3.4) in the $Rig(k) >> 1$ limit gives $E(k) \propto k^{-11/5}$ which is the Bolgiano-Obukhov spectrum. It is thus clear that the exact solution for $g(k)$ obtained by numerically integrating Eq.(3.18) starting at some small value of k with an initially prescribed $g(k)$ will evolve differently for different values of the Richardson number and in the extreme cases $Ri \rightarrow 0$ and $Ri\, g(k) >> 1$ yield the two limiting spectra. The departure from the Kolmogorov region occurs if $Rig(k) > 1$ with $g(k) \propto k^{4/3}$ leading to the constraint $Rik^{4/3} > 1$ which implies that it occurs at wave-numbers $k > Ri^{-3/4}$. We define a wave-number k_B by the relation $k_B = Ri^{-3/4}$ and another wave number k_C by the relation $k_C = Ri^{-3/16}$. The combined conclusion of Secs 2 and 3 is that a clear Bolgiano-Obukhov spectrum can only be seen in the span $k_B < k < k_C$.

4. Discussion of the crossovers

In this section, we use the essential features of the crossover issues in Sections 2 and 3 to write down a handy crossover formula which can be used to analyze experimental and numerical data. To this end, we rewrite Eq.(2.23) as

$$E(k) = \frac{E_0 k^{-11/5}}{\left[1+\left(\frac{k}{k_C}\right)^{8/3}\right]^{4/5}} \qquad \ldots (4.1)$$

where the constant E_0 is dependent on the Richardson number. This provides the crossover from the Bolgiano-Obukhov spectrum to an early dissipative range spectrum. To simplify the Kolmogorov to Bolgiano-Obukhov crossover, we return to Eq (3.18) and simplify it by modifying a couple of inessential details. We carry out approximations in the functional forms involving the square roots to cast everything as a function of the square root $\sqrt{1+Rig(k)}$ alone which leaves the two limiting forms ($Ri<<1, Ri>>1$) unchanged. What this amounts to is that we take Eq.(3.18) and replace the number '6' appearing in two places by the number '4'.This leads us to a much simplified crossover differential equation

$$\frac{dg}{dk}+\frac{4g}{k}=\frac{2^{7/4}}{k^2}\frac{g^{7/4}}{\left[1+Rig(k)\right]^{1/8}} \qquad \ldots (4.2)$$

It is slightly more convenient to work in terms of $h(k)=g^{-3/4}(k)$ and $l=k^{-1}$,which casts Eq.(4.2) in the form

$$\frac{dh}{dl}+\frac{3h}{l}=\frac{\alpha}{(1+Ri/h^{4/3})^{1/8}} \qquad \ldots (4.3)$$

where $\alpha=2^{7/4}$. The above form is easily amenable to perturbation theory for small Richardson numbers and to the lowest non-trivial order

$$h(l)=\frac{\alpha l}{4}-\frac{3\alpha}{64}\left(\frac{4}{\alpha}\right)^{4/3}\frac{Ri}{l^{1/3}}+O(Ri^2) \qquad \ldots (4.4)$$

It is easy to check that for high Richardson numbers the asymptotic form of $h(l)$ is

$$h(l)=\beta l^{6/5} \qquad \ldots (4.5)$$

where β is a function of the Richardson number which vanishes for $Ri\to\infty$. An approximate formula which follows the above constraints is

$$h(l)=\frac{\alpha l}{4}\left(\frac{1}{1+\frac{Ri}{l^{4/3}}}\right)^{3/20} \qquad \ldots (4.6)$$

Remembering $l=1/k$, $g(k)=h(k)^{-4/3}$ and $k_B=Ri^{-3/4}$ we get

$$g(k)=\left(\frac{k}{k_B}\right)^{4/3}\left(1+\frac{k^{4/3}}{k_B^{4/3}}\right)^{1/5} \qquad \ldots (4.7)$$

Now turning to Eq. (3.8) and using the same approximations as explained below Eq. (4.1) , we arrive at the simplest possible crossover as

$$E(k)=K_0\left(\frac{k}{k_B}\right)^{-3}\frac{g(k)}{\sqrt{1+B_0 Ri\, g(k)}} \qquad \ldots (4.8)$$

In the above equation K_0 and B_0 are numerical constants of order unity which should be material independent and hence the above crossover has a universal character. For $Ri << 1$ Eq. (4.8) yields $E(k) \propto g(k)k^{-3}$ and further $g(k) \propto k^{4/3}$ since in this limit $k / k_B << 1$ .The Kolmogorov energy spectrum is obtained for very small Richardson numbers. For $Rik^{4/3} >> 1$, i.e. $k >> k_B$ we crossover to the Bolgiano spectrum. If we want a single formula to represent the crossover to the spectrum for $k >> k_C$, we can combine Eqs (4.8) and (2.25) to write

$$E(k) = K_0 \left(\frac{k}{k_B} \right)^{-3} \frac{g(k)}{\sqrt{1 + Rig(k)}} \frac{1}{\left[1 + \mu \left(\frac{k}{k_B} \right)^{8/3} \right]^{4/5}} \qquad \ldots (4.9)$$

The number μ in the above formula is the ratio $\mu = (k_B / k_C)^{8/3}$ and is expected to be orders of magnitude smaller than unity. The constant B_0 has been set equal to unity which is consistent with the order of accuracy in the approximations in this section. The compensated functions shown in Fig 1 are obtained from Eq.(4.1) with the overall scale-factor set to unity.

The crossovers are now clearly seen. At any given Richardson number *Ri*, for small wave-numbers satisfying $Rik^{4/3} << 1 (k << k_B)$, one gets $E(k) \propto k^{-5/3}$. As the wave-number increases, it begins to crossover to $E(k) \propto k^{-11/5}$ and for $k >> k_B$, it is predominantly of the Bolgiano-Obukhov variety. If the wave-number is increased further to $k >> k_C$, the crossover to a faster decay is obtained as shown in Eq. (2.25) with

$E(k) \propto k^{-13/3}$ before one enters a completely dissipation dominated regime. A function covering the entire range can be written down as

$$E(k)k^{11/5} = \frac{x^{8/15}\left[1+x^{4/3}\right]^{1/5}}{\left[1+Rix^{4/3}\left(1+x^{4/3}\right)\right]^{1/2}}\left[\frac{1}{1+\mu x^{8/3}}\right]^{4/5} \quad \ldots(4.10)$$

For very small Richardson numbers, there is hardly any flat region in the compensated spectrum. It is for Richardson number of order unity that about a decade of flat compensated spectrum is obtained. For higher Richardson number , the anisotropy is expected to play a major role. For $Ri = 1$, our formula yields answers very similar to those seen in Fig ( ) of Ref.(6) and Fig (4b) of Ref.(7). Here it is clearly seen that the spectrum crosses over from Kolmogorov to Bolgiano-Obukhov as the wave-number increases and then departs again both in the calculation here and the simulations.

For completeness, we provide the crossover results in co-ordinate space as well. In co-ordinate space one studies the correlation function $S_2(r) = \left\langle [\mathbf{u}(\mathbf{x}+\mathbf{r}) - \mathbf{u}(\mathbf{x})]^2 \right\rangle$. The relation between $S_2(r)$ and $E(k)$ is obtained as

$$S_2(r) = 4\int_0^\infty E(k)\left[1 - \frac{\sin kr}{kr}\right]dk \quad \ldots (3.26)$$

The energy spectrum $E(k)$ is obtained from Eqs. (3.25) and (3.8) and $S_2(r)$ from Eq.(3.26). The crossover features are as follows. For large values of r corresponding to $r >> Ri^{3/4}$, the spectrum is Kolmogorov i.e $S_2(r) \propto r^{2/3}$, for $r << Ri^{3/4}$ (more precisely $Ri^{5/8}$), the spectrum is

Bolgiano-Obukhov i.e. $S_2(r) \propto r^{6/5}$ and for still smaller r (but still not in the dissipative range) it is $S_2(r) \propto r^{10/3}$ as established by Eq (2.23). This implies that if one observes a Bolgiano-Obukhov spectrum at a certain spatial scale at a low Richardson number, it is possible that one will observe a Kolmogorov spectrum at that same spatial scale at a high Richardson number.

5. Conclusion

We have reviewed the turbulence energy spectrum in stratified fluids and looked at the issue of crossover from Kolmogorov to Bolgiano-Obukhov scaling and beyond in the energy spectrum of a stably stratified fluid (when the results are always true) and in a convecting fluid (when our results hold only if the Bolgiano Obukhov spectrum is numerically or experimentally observed). The key observation is that what determines the crossover from one regime to another is the product k^nRi where n is a number of order unity. For values of k^nRi greater than order unity, it is the Bolgiano-Obukhov spectrum which is relevant and for lower than unity values the observed spectra should be Kolmogorov like. The value of n is 4/3 in the extreme Kolmogorov limit and increases to 8/5 for larger Richardson numbers. At values of k significantly higher than that required for onset of the Bolgiano spectrum, the energy spectrum crosses over to a $k^{-13/3}$ form. In co-ordinate space the second order structure factor which is the Fourier transform of the energy spectrum scales as $r^{2/3}$ at large distance scales (Kolmogorov) and crosses over to a Bolgiano-Obukhov spectrum ($r^{6/5}$) at shorter scales and a $r^{10/3}$ form at even shorter scales bordering on the

dissipative regime. This is seen in Fig (6) of Ref [15] but not mentioned in the article.

References

1. Kolmogorov A. N. The local structure of turbulence in incompressible viscous fluid for very large Reynolds number. *C. R. Acad. Sci.* USSR. **30** 301 (1941)
2. Bolgiano R. Turbulent spectra in stably stratified atmosphere. *J. Geophys. Res.* **64** 2226 (1959)
3. Obukhov A. M. On influence of buoyancy forces on the structure of temperature field in a turbulent flow. *Dokl. Akad. Nauk. SSSR* **125** 1246 (1959)
4. Chandrasekhar S. *Hydrodynamic and Hydromagnetic Stability* Dover Publications (New York) (19)
5. Bhattacharjee J. K. Kolmogorov argument for the scaling of the energy spectrum in a stratified fluid Phys Lett A**379** 696 (2015)
6. Kumar A, Chatterjee A.G. , Verma M.K. Energy spectra of buoyancy driven convection Phys Rev E**90** 023016 (2014)
7. Rosenburg D, Pouquet A, Marino R, Mininni P D Evidence of Bolgiano scaling in rotating stratified turbulence using high resolution direct numerical simulation Phys Fluids **27** 0551055 (2015)
8. Grossmann S; Lohse D. Fourier-Weierstrass mode analysis for thermally driven turbulence. *Phys. Rev. Lett.* **67** 445 (1991)
9. Borue V; Orszag S. A. Turbulent convection driven by a constant temperature gradient. *J. Sci. Comput.* **12** 305 (1997)
10. Kerr R. M. Rayleigh number scaling in numerical convection. *J. Fluid Mech.* **310** 139 (1996)
11. L'vov V. S. Spectra of velocity and temperature-fluctuations with constant entropy flux of fully developed free convective turbulence. *Phys. Rev. Lett.* **67** 687 (1991)

12. Procaccia I; Zeitak R. Scaling exponents in non-isotropic convective turbulence *Phys. Rev. Lett.* **62** 2128 (1992)

13. Calzavarini E; Toschi F; Trippizione R. Evidences of Bolgiano-Obukhov scaling in three dimensional Rayleigh Benard convection. *Phys. Rev. E* **66** 016304 (2002)

14. Brandenberg A. Energy spectra in a model for convective turbulence *Phys. Rev. Lett.* **69** 605 (1992)

15. Kunnen R. P. J; Clerex H. J. H; Geurts B. J; Bokhoven L. J. A; Akermanns R. A. D; Verzico R. Numerical and experimental investigation of structure function scaling in turbulent Rayleigh-Benard convection. *Phys. Rev. E* **77** 016302 (2008)

16. Palimskiy I. B. Numerical investigation of spectrums of turbulent convection. *Izvestiya Atmospheric and Oceanic Physics* **45** 646 (2009)

17. Verma M. K; Kumar A; Pandey A. Phenomenology of buoyancy driven turbulence : recent results. *New J. Phys.* **19** 025012 (2017)

18. Alam S; Guha A; Verma M. K. Revisiting Bolgiano-Obukhov scaling for moderately stably stratified turbulence. *J. Fluid Mech.* **875** 961 (2019)

19. Riley J. J; de Bruyn Kops S. M. Dynamics of turbulence strongly influenced by gravity. *Phys. Fluids* **15** 2047 (2003)

20. Lindborg E. The energy cascade in a strongly stratified fluid. *J. Fluid Mech.* **550** 207 (2006)

21. Herbert D. A; Lindborg E. Relation between vertical shear rate and kinetic energy dissipation rate in stably stratified flows. *Geophys. Res. Lett.* **33** L06602 (2006)

22. Brethouwer G; Billant P; Lindborg E; Chomaz J. M. Scaling analysis and simulation of strongly stratified turbulent flows. *J Fluid Mech.* **585** 343 (2007)

23. Riley J. J; Lindborg E. Stratified turbulence: possible interpretation of some turbulence measurements. *J. Atmos. Sci.* **65** 2416 (2008)

24. Almalkie S; de Bruyn Kops S. M. Kinetic energy dynamics in forced, homogeneous and axisymmetric stably stratified turbulence. *J. Turb.* **13** 29 (2012)

25. Basu A; Bhattacharjee J. K. Kolmogoov or Bolgiano-Obukhov: Universal scaling in stably stratified fluids. *Phys. Rev. E* **100** 033117 (2019)

26. Bhattacharjee J .K. A randomly stirred model for Bolgiano-Obukhov scaling in a stably stratified fluid *Phil. Trans. Roy. Soc.* A**380** 2021007 (2022)

27. Bhattacharjee J. K. Universal crossover from Kolmogorov to Bolgiano-Obukhov scaling in a stably stratified fluid *Phys. Lett.* A **417** 127682 (2021)

28. Chandrasekhar S. On the decay of isotropic turbulence. *Phys. Rev.* **75** 896 1454 (1949)

29. Chandrasekhar S. On Heisenberg's elementary theory of turbulence. *Proc. Roy. Soc. A* **200** 20 (1949)

30. Heisenberg W. On the theory of statistical and isotropic turbulence. *Proc. Roy. Soc. A* **195** 402 (1948)

———————

INDIAN JOURNAL OF THEORETICAL PHYSICS, VOL 70, NOS. 3 & 4, 2022

On MHD Blood Flow Through Permeable Bifurcated Arteries in Tumor Treatments.

Anup Kumar Karak [1] and Ruma Bagchi [2]

Department of Mathematics, Berhampore Girls' College

Berhampore, Murshidabad, West Bengal, Pin - 742101

1 e.mail: karakanup99@gmail.com

2 e.mail: rumabagchi33@gmail.com

(1 Corresponding author.)

[Abstract: Effect of heat transfer on MHD blood flow through an inclined stenosed artery with heat source has been investigated. The viscosity of the blood is assumed to be constant throughout the region of the artery. Analytical solutions of the governing equations have been obtained by treating blood as incompressible conducting Newtonian fluid. Momentum and energy equations of the fluid flow are simplified for mild symmetric stenosis within the artery. Variations of flow rate and shear stress for different values of inclination angle and hematocrit parameter along the diseased part of artery have been shown graphically followed by conclusions.]

Keywords: Stenosis, heat source, Newtonian fluid, symmetric stenosis, shear stress.

1. Introduction

A large number of investigations are in light regarding blood flow through arteries containing various kinds of stenosis. It may be mentioned that the magnetic field reduces the rate of flow of blood in human arterial system, which is useful in the treatment of certain cardiovascular disorders (Korchevskii and Marchounik[1]) as well as in problems concerning with the increasing of the rate of circulation of blood e.g. hemorrhage and hypertension etc. Extensive research works are going on for dynamics of biological fluid in presence of magnetic field for which number of magnetic devices has also been developed for cell separation, drug carriers, cancer tumor treatment etc. Heat transfer in blood is also important to find applications in muscle, skin tissues as well as in thermal therapy etc.

The idea of electromagnetic fields in medical research was due to Kolin[2]. Korchevskii *et al*[1] discussed the possibility of regulating the movement of blood in human system by applying magnetic field. Halder[3] analyzed the effect of magnetic field on blood flow through an indented tube in presence of erythrocytes. A mathematical model for blood flow in magnetic field has been proposed by Tzirtzilakis[4]. Singh and Rathee[5] studied two-dimensional MHD blood flow with variable viscosity through stenotic artery in porous medium. A numerical study of the effect of magnetic field on blood flow in artery having multiple stenoses has been done by Varshney *et al.*.[6]

Now the effect of heat transfer in blood vessels is also important from practical points of view. Barcroft and Edholm[7] studied the effect of temperature on blood flow and deep temperature in the human forearm and also examined the variation of blood motion due to changes in temperature of the surrounding atmosphere. The local temperature effect on blood

flow in human foot was discussed by All wood and Burry.[8] Charm *et al.*[9] investigated experimentally the effect of heat transfer in small tubes of diameter 0.6 mm in a water bath, while Victor and Shah[10] computed heat transfer for uniform heat flux and uniform wall temperature for fully developed flow in the entrance region. The estimation of heat transfer under different configurations and diameters of blood vessels correlation equations were developed by Chato.[11] Lagendijk[12] analyzed temperature distributions in the entrance region around the vessels during hyperthemia. Barozzi and Dumas[13] calculated heat transfer in the entrance region to investigate the rheological properties of the blood stream and cell free peripheral plasma layer at the vessel wall.

Ogulu and Abbey[14] analyzed the simulation of heat transfer on oscillatory blood flow in an indented porous artery while the dynamic response of heat and mass transfer in blood flow through bifurcated arteries under stenotic conditions has been considered by Chakravarty and Sen.[15] Obdulia and Taehong Kim[16] investigated the variations of temperature distributions in an atherosclerotic plaque experiencing an inflammatory process. A dynamical model for heat transfer to blood flow in a small tube was also proposed by Wang.[17]

The present contribution is to find the combined effect of heat transfer and an inclined uniform transverse magnetic field on blood flow through an inclined parallel plate channel with radiation and heat source. The effect of non-dimensional governing parameters on axial flow transport, temperature, concentration profiles and normal velocity have been estimated and presented through graphs.

2. Mathematical Formulation of Problem

From mathematical point of view, the following assumptions are made for the problem:

Blood is Newtonian, incompressible, homogeneous and conducting viscous fluid with constant viscosity. The effect of thermal radiation, chemical reaction, heat source and magnetic field on blood flow is taken into account. Blood flow through the artery under inclined uniform transverse magnetic field and heat transfer is assumed to be of two-dimensional layer.

The flow equations are given as follows:

$$\frac{\partial u^*}{\partial x^*} + \frac{\partial v^*}{\partial y^*} = 0 \qquad \ldots (1)$$

$$\frac{\partial u^*}{\partial t^*} + \nu \frac{\partial u^*}{\partial y^*} + \frac{1}{\rho}\frac{\partial p^*}{\partial x^*}$$

$$= \nu \frac{\partial^2 u^*}{\partial y^{*2}} - \left[\frac{\sigma B_0^2 \cos^2\alpha}{\rho}\right] u^* + g\beta_T (T - T_\infty)^* + g\beta_c (C - C_\infty)^* \qquad \ldots (2)$$

$$\frac{\rho C_p}{K_T}\left[\frac{\partial T^*}{\partial t^*}\right] + \nu \frac{\partial T^*}{\partial y^*} = \frac{\partial^2 T^*}{\partial y^{*2}} + \frac{Q}{K_T}(T - T_\infty)^* - \frac{\partial q_r^*}{\partial y^*} \qquad \ldots (3)$$

$$\frac{\partial C^*}{\partial t^*} + \nu \frac{\partial C^*}{\partial y^*} = D \frac{\partial^2 C^*}{\partial y^{*2}} - K_r^* (C^* - C_\infty) \qquad \ldots (4)$$

The thermal radiation heat flux q_r^* by using Rosseland's approximation is expressed as

$$q_r' = -\frac{4\delta'}{3k'}\frac{\partial T'}{\partial y'} = -\frac{4\delta'}{3k'}\nabla T'$$

where δ^* is the Stefan-Boltzmann constant and k^* is the Rosseland mean absorption coefficient. Assuming that the temperature differences within the

flow are sufficiently small so that T^* may be expressed as a linear function of temperature in the form

$$T^* = 4T_0^3T - 3T_0^*$$

This implies that

$$q_r^* = -\frac{16\delta^*T_0^3}{3k^*}\frac{\partial T}{\partial y} \quad \ldots (5)$$

The higher order terms in the expansion (Tailors series expansion) in T_0^* is neglected

In the above equations, u^* and $v^*$are the vertical and horizontal component velocities in the x^* and y^* direction respectively, α is the angle of inclination of the magnet field, t^* is the time, T^* is the temperature, θ^* is the temperature distribution and g is the acceleration due to gravity, B_0 is the constant magnetic field, C_p is the specific heat capacity, M is the magnetic parameter. Pr is the Prandtl number, ρ is the density of the blood, β_T is the coefficient of volume expansion due to temperature and β_c is the coefficient of volume expansion due to concentration, σ is the electrical conductivity, K_r is the chemical reaction parameter, R is the radiation parameter, S_c is the Schmidt number, S is the heat source and m is the rate of mass flow, λ is the decay parameter, c^* is the chemical concentration, D is the diffusion coefficient.

We introduce the following non-dimensional quantities for convenience:

$$y = \frac{y^*}{b};\ x = \frac{x^*}{b};\ t = \frac{\nu t^*}{b^2}\quad u = \frac{2\rho b}{m}u^*;\ \ \theta = \frac{2\rho b^3}{\nu m}(T - T_\infty)^*;$$

$$C = \frac{2\rho b^3}{\nu m}(C - C_\infty)^*;$$

$$h(x,t) = \frac{2b^3}{\nu m}\frac{\partial p^*}{\partial x^*};\ M = \frac{\sigma B_0^2 b^2}{\nu};\ K = \frac{K_r^* b^2}{\nu};\ R = \frac{16\delta^* T_0^2}{3k^* k};$$

$$\nu = \frac{\mu}{\rho};\ P_r = \frac{\mu C_p}{K_T};\ S_c = \frac{\nu}{D}; s = \frac{Qb^2}{k} \quad \ldots(6)$$

The continuity, momentum, energy and diffusion equation in dimensionless from are then read as follows:

$$\frac{\partial u}{\partial x} + \frac{\partial u}{\partial y} = 0 \quad \ldots(7)$$

$$\frac{\partial u}{\partial t} + b\frac{\partial u}{\partial y} + h(x,t) = \frac{\partial^2 u}{\partial y^2} - (Mcos^2\alpha)u + g\beta_T\theta + g\beta_c C \quad \ldots(8)$$

$$P_r\frac{\partial \theta}{\partial t} + P_r b\frac{\partial \theta}{\partial y} = (P_r + R)\frac{\partial^2 \theta}{\partial y^2} + S\theta \quad \ldots(9)$$

$$S_c\frac{\partial C}{\partial t} + S_c b\frac{\partial C}{\partial y} = \frac{\partial^2 C}{\partial y^2} - S_c K_r C \quad \ldots(10)$$

3. Solution of the Problem

The boundary conditions for the problem in non-dimensional form are:

$$u = e^{-\lambda^2 t}, \quad \theta = e^{-\lambda^2 t}, \quad C = e^{-\lambda^2 t}, \quad \text{at } y = -1$$

$$u = 0, \quad \frac{\partial \theta}{\partial y} = 0, \quad C = 0, \quad \text{at } y = 1 \quad \ldots(11)$$

Let us choose

$$u(y,t) = F(y)e^{-\lambda^2 t} \quad \ldots(12)$$

$$v(y,t) = A(y)e^{-\lambda^2 t} \quad \ldots(13)$$

$$\theta(y,t) = G(y)e^{-\lambda^2 t} \quad \ldots(14)$$

$$C(y,t) = H(y)e^{-\lambda^2 t} \quad \ldots(15)$$

Substituting (12) - (15) into equations (7) - (10) we got

$$\frac{\partial F}{\partial x} + \frac{\partial A}{\partial y} = 0 \Rightarrow A = constant,$$

$$\frac{\partial^2 F}{\partial y^2} - b\frac{\partial F}{\partial y} + (\lambda^2 - Mcos^2\alpha)F$$

$$= -g\beta_T G - g\beta_c H + A_3 \ \left[A_3 = he^{\lambda^2 t}\right] \quad \ldots(16)$$

$$(P_r + R)\frac{\partial^2 G}{\partial y^2} - P_r b\frac{\partial G}{\partial y} + (S + P_r\lambda^2)G = 0 \quad \ldots(17)$$

$$\frac{\partial^2 H}{\partial y^2} - S_c b\frac{\partial H}{\partial y} + (S_c\lambda^2 - S_c k_r)H = 0 \quad \ldots(18)$$

And the boundary conditions are

$$F = 1; \quad G = 1; \quad H = 1; \qquad \text{at } y = -1 \quad \ldots(19)$$

$$F = 0; \quad \frac{\partial G}{\partial y} = 0; \quad H = 0 \qquad \text{at } y = 1 \quad \ldots(20)$$

Solving (18) we get

$$H = C_1 e^{m_1 y} + C_2 e^{m_2 y}$$

$$\text{i.e. } C(y,t) = (C_1 e^{m_1 y} + C_2 e^{m_2 y})e^{-\lambda^2 t} \quad \ldots(21)$$

Using boundary conditions we get

$$C_1 = \frac{m_2 e^{m_2}}{e^{m_2 - m_1}(m_2 - m_1 e^{-1})}, C_2 = -\frac{m_1 e^{m_1}}{e^{m_2 - m_1}(m_2 - m_1 e^{-1})}$$

where

$$m_1 = \frac{S_c b + \sqrt{S_c^2 b^2 - 4(S_c\lambda^2 - S_c k_r)}}{2}, m_2$$

$$= \frac{S_c b - \sqrt{S_c^2 b^2 - 4(S_c\lambda^2 - S_c k_r)}}{2}$$

Solving (17) we get

$$G = C_3 e^{m_3 y} + C_4 e^{m_4 y}$$

$$\text{i.e. } \theta(y,t) = (C_3 e^{m_3 y} + C_4 e^{m_4 y}) e^{-\lambda^2 t} \quad \ldots (22)$$

Using boundary conditions we get

$$C_3 = \frac{e^{m_4}}{e^{m_4 - m_3}(1-e^{-1})}, \quad C_4 = -\frac{e^{m_3}}{e^{m_4 - m_3}(1-e^{-1})}$$

where

$$m_3 = \frac{P_r L + \sqrt{P_r^2 b - 4(P_r+R)(S+P_r\lambda^2)}}{2(P_r+R)}, \quad m_3 = \frac{P_r L - \sqrt{P_r^2 b - 4(P_r+R)(S+P_r\lambda^2)}}{2(P_r+R)}$$

Solving (16) we get

$$F = C_5 e^{m_5 y} + C_6 e^{m_6 y} - g\beta_T C_3 \frac{e^{m_3 y}}{m_3^2 - bm_2 + \sigma} - g\beta_T C_4 \frac{e^{m_4 y}}{m_4^2 - bm_4 + \sigma}$$
$$- g\beta_C C_1 \frac{e^{m_1 y}}{m_1^2 - bm_1 + \sigma} - g\beta_c C_2 \frac{e^{m_2 y}}{m_2^2 - bm_2 + \sigma} + \frac{A_3}{\sigma}$$

Using boundary conditions we get

$$C_5 = \frac{\begin{matrix} -d_1 e^{2m_3 - m_6} + d_2 e^{2m_4 - m_6} - d_3 e^{2m_1 - m_6} + d_4 e^{2m_2 - m_6} + d_5 e^{-m_6} \\ + d_1 e^{m_6} - d_2 e^{m_6} + d_3 e^{m_6} - d_4 e^{m_6} - d_5 e^{m_6} + e^{m_6} \end{matrix}}{e^{m_6 - m_5} - e^{m_5 - m_6}}$$

$$C_6 = \frac{\begin{matrix} -d_1 e^{m_5} + d_2 e^{m_5} - d_3 e^{m_5} + d_4 e^{m_5} + d_5 e^{m_5} - e^{m_5} + d_1 e^{2m_3 - m_5} \\ - d_2 e^{2m_4 - m_5} + d_3 e^{2m_1 - m_5} - d_4 e^{2m_2 - m_5} - d_5 e^{-m_5} \end{matrix}}{e^{m_6 - m_5} - e^{m_5 - m_6}}$$

where

$$d_1 = \frac{g\beta_T m_4}{(m_4 - m_3 e^{-1})(m_3^2 - bm_3 + \sigma)}, d_2$$
$$= \frac{g\beta_T m_3}{(m_4 e^{-1} - m_3)(m_4^2 - bm_4 + \sigma)}, d_3$$

$= \frac{g\beta_c}{(1-e^{-1})(m_1^2-bm_1+\sigma)}, d_4 = \frac{g\beta_c}{(e^{-1}-1)(m_2^2-bm_2+\sigma)},\ d_5 = \frac{A_3}{\sigma}$.

i.e.

$$u(y,t) = \left(C_5 e^{m_5 y} + C_6 e^{m_6 y} - g\beta_T C_3 \frac{e^{m_3 y}}{m_3^2-bm_2+\sigma} - g\beta_T C_4 \frac{e^{m_4 y}}{m_4^2-bm_4+\sigma} - g\beta_C C_1 \frac{e^{m_1 y}}{m_1^2-bm_1+\sigma} - g\beta_C C_2 \frac{e^{m_2 y}}{m_2^2-bm_2+\sigma} + \frac{A_3}{\sigma}\right) e^{-\lambda^2 t} \quad \ldots (23)$$

4. Results & discussions

The numerical results of axial velocity, normal velocity and temperature obtained from the above analysis are shown graphically for different values of magnetic field parameter (M), Prandtl number (Pr) and heat source parameter (S) against y for better understanding of the problem.

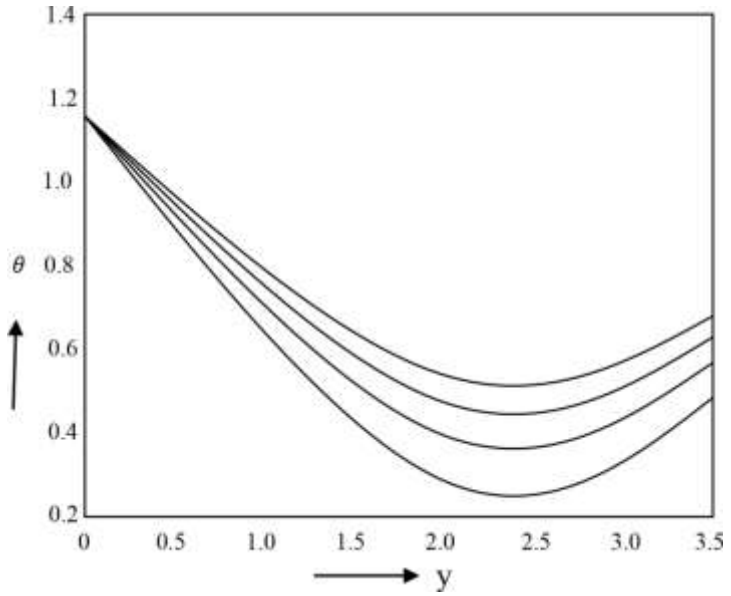

Fig. 1. Temperature distribution for different values of Heat source parameter (S)

Figure 1 illustrates the behavior of temperature field at t = 1, λ = 0.2, b = 0.2, Pr = 0.5 and for different values for heat source parameter (S = 1,

1.5, 2, 2.5). It is observed that the temperature decreases with increasing the values of the heat source upto $y \leq 2.4$ but increases from $y \geq 2.4$ for different values of S.

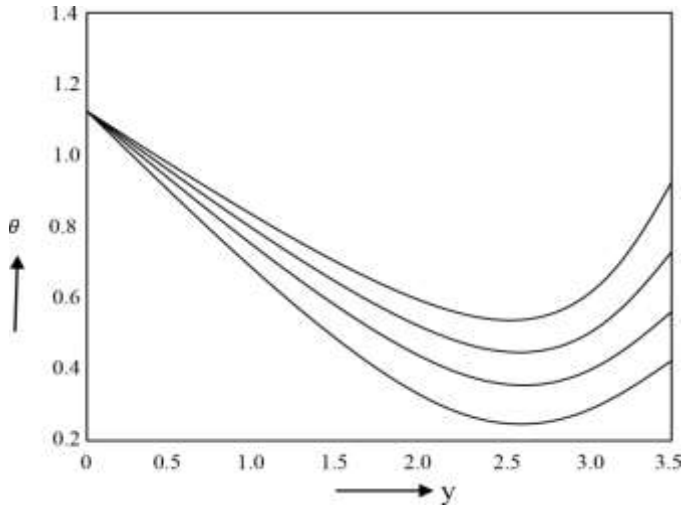

Fig. 2. Temperature distribution for different values of Prandtl number (Pr).

Figure 2 describes the effect of different values of Prandtl number (Pr = 0.5, 1.5, 2.5, 3.5) at t = 1, $\lambda = 0.2$, b = 0.2, S = 1.5. The effect of Prandtl number on temperature is same as heat source parameter. It is decreasing with increasing the values of Parndtl number upto $y \leq 2.5$ but reverse effect is observed for $y \geq 2.5$ (for different values Pr).

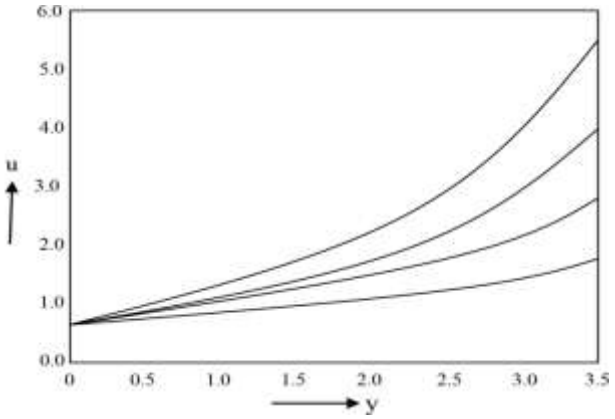

Fig. 3. Axial velocity for different values of Magnetic field parameter M.

From figure 3, we note that axial velocity of blood is increasing for increasing values of magnetic field parameter (M), when heat source parameter(S) is kept constant at(S=5). For M=1.6, the axial velocity is increasing very fast against y while for M=1 the velocity increases slowly.

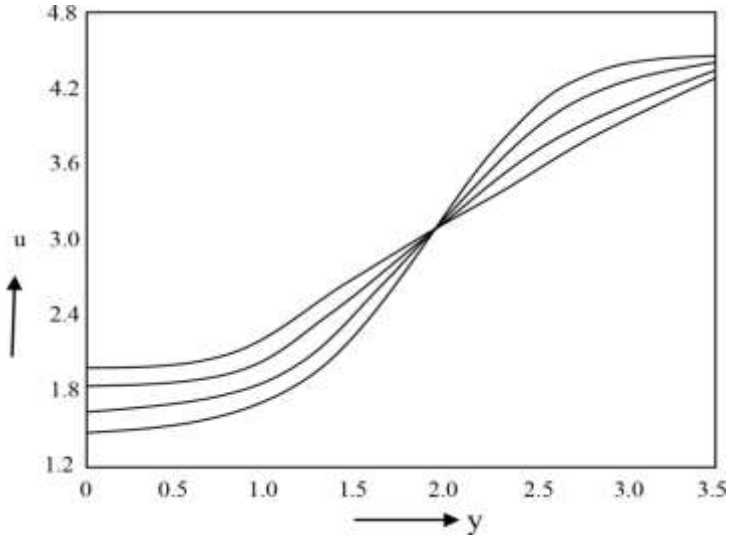

Fig. 4. Axial velocity for different values of heat source parameter (S)

Figure 4 indicates the effect of heat source parameter (S) on axial velocity of blood against y. It is clear that the velocity increases with increasing values of heat source parameter(S) for $y \leq 2.0$ and represents reverse effect for $y \geq 2.0$.

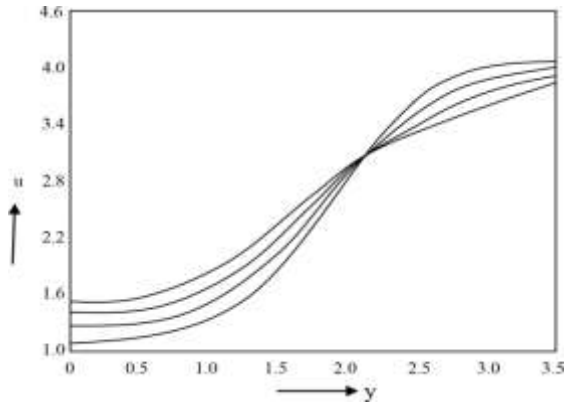

Fig. 5. Axial velocity for different values of Prandtl number.

Axial velocity for different values of Prandtl number (Pr) is shown in Fig. 5. From Fig. 5, we conclude that the velocity is increasing for increasing values of Pr for $y \leq 2.2$ and decreasing for the same values of Pr for $y \geq 2.2$.

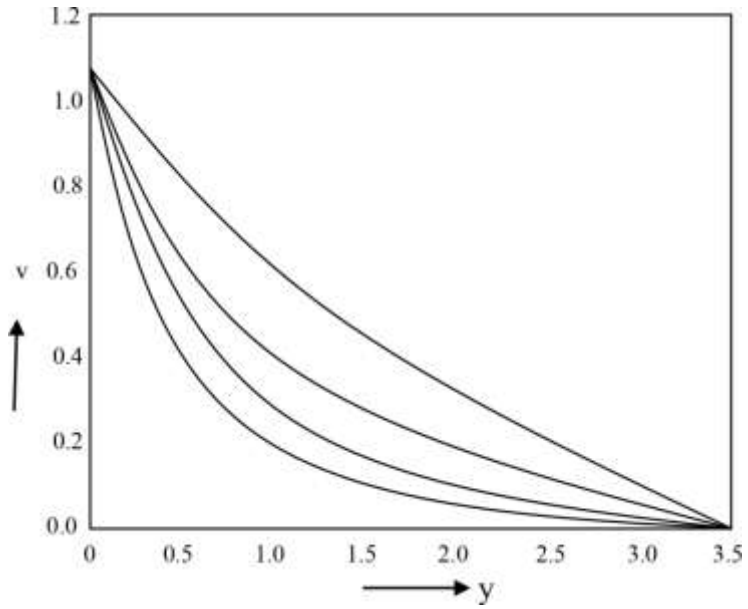

Fig. 6. Normal velocity for different values of decay parameter (λ)

It is also clear from the fig.6 that the normal velocity is decreasing with increasing values of λ and also for increasing values of t. The velocity is decreasing slowly for λ= 1 while it is tending to zero very fast for λ= 2.5. It is due to the velocity is exponential function

5. Conclusions:

The impacts of thermal radiation, chemical reaction, and heat source on unsteady MHD blood flow through an artery with an angled magnetic field are investigated including other factors.

An increase in the magnetic field causes both blood flow and volumetric blood flow rate through the artery to decrease. This process can treat low blood pressure by raising blood pressure to return to normal. Sickle cell patients can also be treated by improving blood flow and maintaining oxygen in the hemoglobin as a result of increased blood flow when the magnetic field decreases. This can reduce strokes, swelling and pain when affected areas are exposed to the magnetic field at different tilt angles.

As the intensity of the magnetic field parameter (M), thermal radiation (R), and chemical reaction parameters increases, the blood flow rate also decreases. For high blood pressure problems it can be treated well with repeated and accurate clinical dosing.

Increasing the thermal radiation parameter decreases blood flow while the volumetric blood flow rate increases. This is due to the blood vessels narrowing (lesion), resulting in a reduction in blood flow through the vessels. This approach can also be used to treat tumors. Increased thermal radiation causes a decrease in blood temperature, which shrinks tumor growth in the area of exposure.

Increasing the heat source increases blood flow, the volumetric flow rate of blood, and raises the temperature of blood. This can lead to cramps and sometimes death.

An increase in permeability reduces both blood flow and volumetric blood flow, and an increase in the inclination angle of the magnetic field reduces blood flow near the arterial wall but decreases blood flow away from the wall.

Decreases in normal speed significantly is to reduce damping parameter.

A carotid artery containing a tumor is concentrated by drug whose concentration increases for large Schmidt number while decreases for large reaction parameter. This gives a multiple therapy if approved by medical persons.

References

1. E. M. Korchevskii, L. S. Marochnik, "Magnetohydrodynamic version of movement of blood", Biophysics, **10**, pp. 411–413 (1965).
2. A. Kolin, "An electromagnetic flow meter: Principle of the method and its application to blood flow measurements", Proc. Soc. exp. Biol. (N. Y.), **35,** pp. 53-56 (1936).
3. K. Halder, "Effect of a magnetic field on blood flow through an indented tube in the presence of erythrocytes", Indian Journal of Pure and Applied Mathematics, **25(3)**, pp. 345-352 (1994).
4. E. E. Tzirtzilakis, "A mathematical model for blood flow in magnetic field", Physics of Fluids, **17**, pp. 077103 (2005).
5. J. Singh, R. Rathee, "Analytical solution of two-dimensional model of blood flow with variable viscosity through an indented artery due to LDL effect in the presence of magnetic field", International Journal of the Physical Sciences, **5(12)**, 4, pp. 1857-1868 (2010).
6. S. A. Victor, V. L. Shah, "Heat transfer to blood flowing in a tube", Biorheology, **12**, pp. 361-368 (1975).
7. H. Barcroft, O. G. Edholm, "The effect of temperature on blood flow and deep temperature in the human forearm", J. Physiol, **102**, pp. 5-20 (1942).
8. M. J. Allwood, H. S. Burry, "The effect of local temperature on blood flow in the human foot", J. Physiol, **124(2)** , pp. 345-357 (1954).
9. S. Charm, B. Paltiel, G. S. Kurland, "Heat transfer coefficients in blood flow", Biorheology, **5**, pp.133-145 (1968).

10. C. Y. Wang, "Heat transfer to blood flow in a small tube", J Biomech Eng., **130(2)**, pp.024501 (2008).

11. J. C. Chato, "Heat transfer to blood vessels", Transc. ASME, **102**, pp. 110-118 (1980).

12. J. W. Lagendijk, "The influence of blood flow in large vessels on the temperature distribution in hyperthermia", Phys. Med. Biol. **27**, pp. 17-82 (1982).

13. G. S. Barozzi, A. Dumas, "Convective heat transfer coefficients in the circulation", Journal of Biomech. Eng., **113**, issue 3, pp. 308-313 (1991).

14. A. Ogulu, T. M. Abbey, "Simulation of heat transfer on an oscillatory blood flow in an indented porous artery", International communication in heat and mass transfer, **32**, issue 5, pp. 983-989 (2005).

15. S. Chakravarty, S. Sen, "Dynamic response of heat and mass transfer in a blood flow through stenosed bifurcated artery", Korea-Austria Rheology Journal, **17**, no.2, pp. 47-62 (1996).

16. L. Obdulia, K. Taehong, "Calculation of arterial wall temperature in atherosclerotic arteries: effect of pulsatile flow, arterial flow, arterial geometry and plaque structure", Journal of Biomech. Eng., pp. 1186-1475 (2007).

17. M. Zamir, M. R. Roach, "Blood flow downstream of a two dimensional bifurcation", **J.Theo. Biol.,** pp. 33-42 (1973)

18. P. K. Suri, P. R. Suri, "Effect of Static Magnetic field on blood flow in a branch", Indian Journal of Pure and Applied Mathematics, **12(7),** pp. 907-918 (1981).

19. G. Varshney, V. K. Katiyar, S. Kumar, "Effect of magnetic field on the blood flow in artery having multiple stenosis: a numerical study", International Journal of Engineering, Science and Technology, **2**, No. 2, pp. 67-82 (2010).

———————

INDIAN JOURNAL OF THEORETICAL PHYSICS, VOL 70, NOS. 3 & 4, 2022

A Brief Review on Metallic Nanoparticles

Subhendu Chandra

Associate professor in Physics

Victoria Institution (College)

78-B, A. P. C. Road, Kolkata-700 009

[Abstract: Metallic nanoparticles have involved scientist for over a century and are now deeply applied in biomedical sciences and engineering. They are an attention of interest because of their enormous potential in nanotechnology. Today these materials can be synthesized and improved with various chemical functional groups which allow them to be conjugated with antibodies, ligands, and drugs of interest and thus introducing a extensive variety of potential applications in biotechnology, magnetic separation, targeted drug delivery, and automobiles for gene and drug delivery and more significantly diagnostic imaging. Moreover, different imaging modalities have been established over the period of time such as Magnetic resonance imaging (MRI), computed tomography (CT), Positron Emission Tomography (PET), ultrasound, Surface Enhanced Raman Spectroscopy (SERS), and optical imaging as an aid to image various disease states. This led to the invention of various nanoparticulated contrast agent such as magnetic nanoparticles (Fe_3O_4), gold, and silver nanoparticles for their application in these imaging modalities. In addition, to use various imaging techniques in tandem newer multifunctional nanoshells and nanocages have been developed. Thus in this review article, we aim to provide an introduction to magnetic nanoparticles

(Fe_3O_4), gold nanoparticles, nanoshells and nanocages, and silver nanoparticles followed by their synthesis, physiochemical properties, and citing some recent applications in the diagnostic imaging and therapy of cancer].

Key word: Metallic, Nanoparticles, SERS, plasmon, imaging

1. General Introduction to Nanoparticles:

Nanoparticles are the simplest form of structures with sizes in the nanometer range. In principle any collection of atoms bonded together with a structural radius of < 100 nm can be considered a nanoparticle[1]. Nanotechnology is the science that deals with material at the scale of 1 billionth of a meter (i.e., 10^{-9} m = 1 nm), and is also the study of manipulating matter at the atomic and molecular scale. A nanoparticle is far smaller than the world of everyday objects that are described by Newton's laws of motion, but bigger than an atom or a simple molecule that are governed by quantum mechanics. In general, the size of a nanoparticle spans the range between 1 and 100 nm. The properties of many conventional materials change when formed from nanoparticles. This is typically because nanoparticles have a greater surface area per weight than bigger particles which causes them to be more reactive to some other molecules. Metallic nanoparticles have different physical and chemical properties from bulk metals (e.g., lower melting points, higher specific surface areas, specific optical properties, mechanical strengths, and magnetizations), properties that might prove attractive in various industrial applications. However, how a nanoparticle is viewed and is defined depends very much on the specific application. The optical phenomenon is one of the essential attractions and a characteristic of a nanoparticle. For example, a 20-nm gold nanoparticle has a characteristic wine red color[2]. A silver nanoparticle is yellowish gray. Platinum and palladium nanoparticles are

black. Not amazingly, the optical characteristics of nanoparticles have been used from time immemorial in sculptures and paintings even before the 4th century AD. The strength of soluble gold was based generally on its remarkable medicinal powers of different diseases like, dysentery, heart and venereal diseases, epilepsy, and tumors etc. The record of the nanoparticle from ancient times to the middle ages has been summarized by Daniel and Astruc[3].

The first book on colloidal gold was published in 1618 by the philosopher and medical doctor Francisci Antonii.[4] This book includes considerable information on the formation of colloidal gold sols with their medical uses and successful practical cases. The book noted that soluble gold appeared around the 5^{th} or 4^{th} century B.C. in Egypt and China. On the other hand, industrial manufacturing of stained glass with colloidal particles was established by Kunckel in the seventeenth century (1676)[5]. He also published a book whose Chapter 7 was concerned with "drinkable gold that contains metallic gold in a neutral, slightly pink solution that exerts curative properties for several diseases". He concluded that gold must be present in aqueous gold solutions to a degree of contamination such that it is not visible to the human eye. A dye in glasses, that is, the "Purple of Cassius", was a colloid resulting from the presence of gold particles and tin dioxide and was highly popular in the 17^{th} century. A complete article on colloidal gold was published in 1718 by Helcher[6]. In the article, this philosopher and doctor stated that the use of boiled starch in its drinkable gold preparation noticeably enhanced its stability. These ideas were common in the 18^{th} century, as indicated in a French chemical dictionary in 1769, under the title "or potable". In 1857, Michael Faraday reported the formation of deep red solutions of colloidal gold by reduction of an aqueous solution of chloroaurate ($AuCl_4^-$) by phosphorus in CS_2[7]. He also investigated the

optical properties of thin films prepared from dried colloidal solutions and observed reversible color changes of the films upon mechanical compression (from bluish-purple to green).

The present technology that deals with nanoparticles, or simply nanotechnology, began from the particular optical observable fact and the establishment of a theory to explain the different physical phenomena that were followed subsequent to the development of analytical instruments.

The latest development of nanoparticles is due to a combination of theory and experiments in the fields of physics, chemistry, materials science, and biosciences. Specific phenomena (chemical properties and physical properties), other than the optical property of a nanoparticle, have led to new possibilities in various fields. Applications of nanoparticles in various fields involve an economical and easy method of synthesizing high quality shaped nanoparticles. For this reason of high quality nanoparticles can be achieved by simple operations compared with the more conventional nanoparticle synthetic methods.

2. Surface Plasmon Resonance and Coloring

The physical properties of surface plasmon resonance (SPR) were reported by Wood who might identify semi-monomolecular coverage[8]. Wood also discovered the plasmon resonance phenomenon would change with the composition of the liquid in contact with the metal surface. He observed a pattern of "anomalous" dark and light bands in the refracted light when he shone polarized light on a mirror with a diffraction grating on its surface. The first theoretical treatment of these anomalies was put forward by Rayleigh in 1907. Rayleigh's "dynamical theory of the grating" was based on an expansion of the scattered electromagnetic field in terms of outgoing waves only. With this assumption, he found that the scattered field was

singular at wavelengths for which one of the spectral orders emerged from the grating at the grazing angle. He then observed that these wavelengths, which have come to be called the Rayleigh wavelengths, λ_R, correspond to the Wood anomalies. Further corrections were made by Fano but a complete explanation of the phenomenon was not possible until 1968[9] when Otto and in the same year Kretschmann and Raether, reported the excitation of the surface plasmon band [10]. In this section they present a basic outline of the relation between surface plasmon resonance and the color of nanoparticles[11].

In solid state physics, the plasmon represents the collective oscillation of a free charge in a metal and may be considered as a kind of plasma wave [12]. The positive electrical charge in the metal is fixed and the free electron is free to move around it. An applied external electric field, as from a light source, causes the free electrons at the surface of the metal to vibrate collectively, giving rise to surface plasmons. Since electrons are also particles with an electric charge, when they vibrate they also generate an electric field, and when the electric field from the vibration of free electrons and the applied external electric field (e.g., electromagnetic waves) resonate the resulting phenomenon is referred to as a surface plasmon resonance that takes place at the surface of the metal. However, if light irradiates a solution that contains dispersed metal nanoparticles smaller than the wavelength of light, then depending on the electric field of light, the deviation produces a free electron at the surface of the metal. As a result, the weak or thick portions of the electric field appear on the nanoparticle surface and can be considered as a kind of polarization. Such localized plasmon resonance is called localized surface plasmon resonance (LSPR)[13]. The LSPR is typically concentrated in a very narrow region on the surface of a nanoparticle. The wavelength corresponding to the LSPR depends on the kind of metal, the

shape of the metal nanoparticle, and the extent of aggregation of the metallic nanoparticles. Moreover, the surface plasma vibration also changes with the dielectric constant and the quality of the carrier fluid. The plasma oscillations in the metal occur mainly in the ultraviolet (UV) region[14].

However, in the case of Au, Ag, and Cu, the plasma shifts nearer to the visible light domain with the band due to electrons in the s atomic orbital. For example, the wavelength of the surface plasmon resonance band maximum of a spherical Au nanoparticle is 520–550 nm[15].

If a colloidal Au nanoparticle solution is now irradiated with visible light at these wavelengths (520–550 nm), the visible light corresponding to the green color is absorbed and the particles now display a red purple color, which is the complementary color to green. In a colloidal Ag nanoparticle solution which has a plasmon resonance band maximum near 400 nm, the blue color of the visible light is absorbed and the Ag particles now take on a yellow color, the complementary color to blue.

3. Size Control of Nanoparticles

The physical and chemical properties of nanomaterials depend not only on their composition but also on the particle size and shape. Accordingly, a high quality synthesis protocol must first of all provide control over particle size and shape. For example, if the diameter of an Au nanosphere is made to increase, the surface plasmon resonance will be gradually shifted from 530 nm to the longer wavelength side. Thus, if nanoparticles differ in size, their optical characteristics will also change significantly[16].

In optical applications of nanoparticles, simplification of the size distribution of the particles becomes a very important factor. Therefore, it is important to fabricate nanoparticles with a single target size in mind.

Generally, in order to prepare mono- dispersed nanoparticles, it is essential that the nanoparticles grow very slowly after the rapid generation of the seed particles. If the size of the nanoparticles decreases (i.e., increase in specific surface area), then the increase in the surface energy of such nanoparticles will make possible their aggregation. Consequently, after their growth to the desired optimal size, it will be necessary to stabilize the particulate surface by addition of a dispersing agent. However, where the concentration of nanoparticles is unusually high, the decentralized stabilization will fall, because the protective action of the organic substrate (citrate) is no longer strong enough to prevent aggregation.

It is important to realize that the physical properties of a nanoparticle can change with the aggregation ratio, even though the colloidal solution may contain nanoparticles of identical size. Methods to separate out particles of a given target size from a colloidal solution which contains nanoparticles of various sizes are known. They are (i) separation by precipitation, (ii) centrifugal separation, (iii) gel filtration column, and (iv) gel electrophoresis. As a feature of each screening method, the precipitation separation is suitable for a large distribution of colloid nanoparticles in the solution. The centrifugal separation and the gel filtration column are well suited for solutions of colloidal nanoparticles with a narrow size distribution. Gel electrophoresis is a suitable method to separate nanoparticles taking advantage of the difference in charge density of the particles, and is suitable for separating particles with a small cluster size. In fact, a combination of these various methods might prove beneficial. However, a problem with sorting the various sized nanoparticles using these methods is that only a fraction of the nanoparticles of a given size may be collected, and then only in small quantities. The digestive ripening method

and high temperature melting technique have been proposed to resolve this problem.

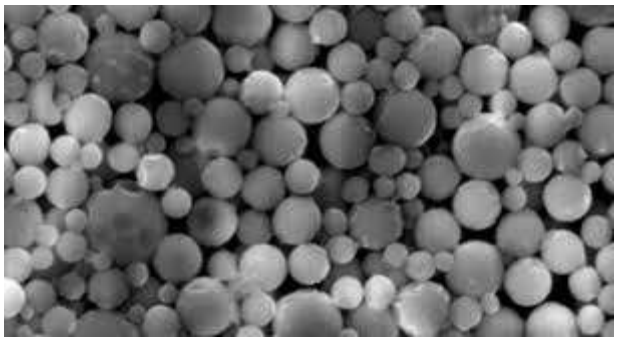

Various sizes of spherical gold nanoparticles

4. Shape Control of Nanoparticles

The shape of nanoparticles is an important factor that determines the nature of the surface plasmon resonance band just as the size of the nanoparticles did. Absorption spectra in the visible spectral region of various Au rod shaped nanoparticles (i.e., nanorods) with changes in the aspect ratio (length : diameter). The diameters of the Au nanorods espousing a pillar form and used in this experiment ranged from 5 to 20 nm and the lengths from 20 to 150 nm[17].

It is worth noting that the change in the ratio of a nanorod is related to the size ratio of a crystal face. An increase in the size ratio (aspect ratio) shifts the maximal absorption band to longer wave lengths. Therefore, the physical composition of the nanorods can easily change their spectroscopic features, such that various studies have been required to understand these characteristics.

In the case of noble metal nanoparticles such as Ag, Au, Pt, and Pd, this shape dependence is particularly evident. For example, Ag and Au nanocrystals of different shapes hold unique optical scattering responses. Whereas highly symmetric spherical particles reveal a single scattering

peak, anisotropic shapes such as rods, triangular prisms, and cubes exhibit multiple scattering peaks in the visible wavelengths due to highly localized charge polarizations at corners and edges. Controlling nanocrystal shape thus provides an elegant approach for optical tuning. Similarly, chemical reactivity is highly dependent on surface morphology. The bounding facets of the nanocrystal, the number of step edges and twist sites, as well as the surface area to volume ratio can dictate unique surface chemistries. For this reason, Pt and Pd nanocrystals exhibit shape and size dependent catalytic properties that may prove useful in achieving highly selective catalysis. Optimizing nanocatalyst morphology has become a successful area of investigation. These thrilling possibilities have raised the key question: can we logically control nanocrystal shape and surface morphology?

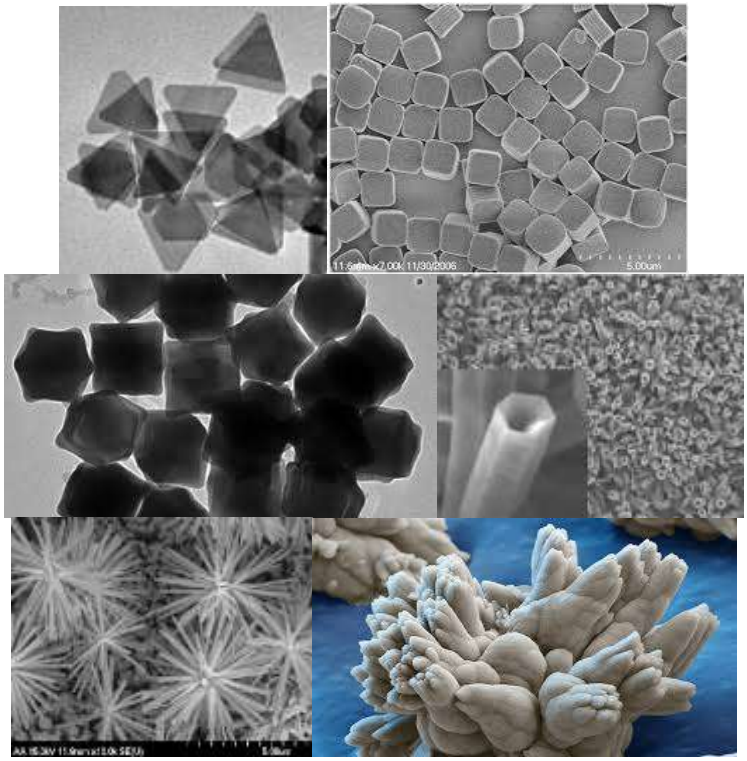

Different shaped nanoparticles [From the left (i) nanoprism (ii) nanocube (iii) nanopyramid (iv) nanorod (v) nanoflower (vi) nanogrowth]

5. Structure Control of Nanoparticles

Nanoparticles that are composed of two or more metals differ in their catalytic, magnetic, and optical characteristics from nanoparticles that consist of a single metal. Such nanoparticles can be sub-divided into three kinds of structures: (i) the alloy structure that exists randomly in a crystal (ii) the core–shell structure in which the metal at the center differs from the peripheral metal and (iii) the twinned hemisphere structure wherein two sorts of hemispheres are joined. The latter heterojunction structure facilitates phase separation. Nanostructures consisting of complex metal nanoparticles tend to hide the various new features. The core–shell structure is comparatively easy to fabricate in complex metal nanoparticles with effective functional control. For instance, although the color of an Au nanoparticle liquid dispersion is purplish red (the purple of Cassius) and that of an Ag nano- particle liquid dispersion appears yellow, whenever Au forms the core and Ag the shell the structure then takes an orange color. Moreover, if a structured matter has magnetic properties, such as magnetite nanoparticles, then the magnetic metal particles could be used to form the structure's core, such that the structure will now be embodied with both magnetic and optical characteristics[18].

Synthetic methods of preparing core–shell nanoparticles are roughly divided into two categories: (i) involving a simultaneous reduction reaction and (ii) involving a sequential one electron reduction reaction. As an example of the simultaneous reduction reaction, consider the core being made up of Pt nanoparticles and the shell composed of Pd nanoparticles. A unique method that uses differences in the oxidation potentials of Ag and Au has also been reported. Here, a silver nanoparticle is added to $HAuCl_4$ solution, following which an oxidation–reduction reaction takes place

wherein gold is deposited on the surface of an Ag nanoparticle yielding the core–shell structure.

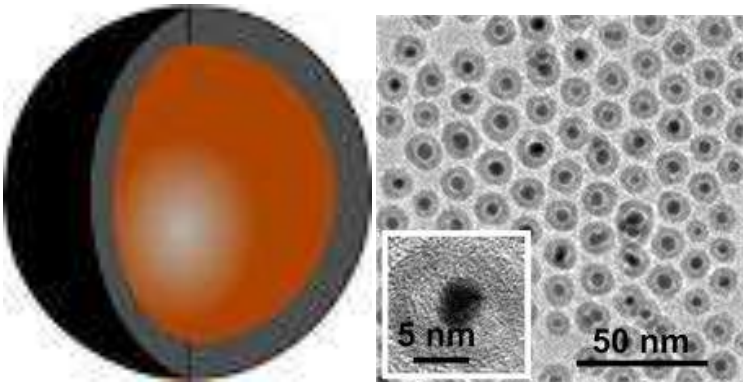

Core-Shell nanoparticle

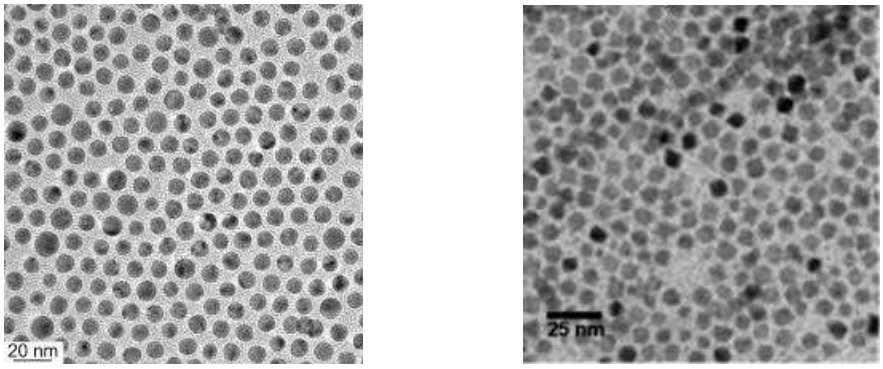

Alloy structured nanoparticle

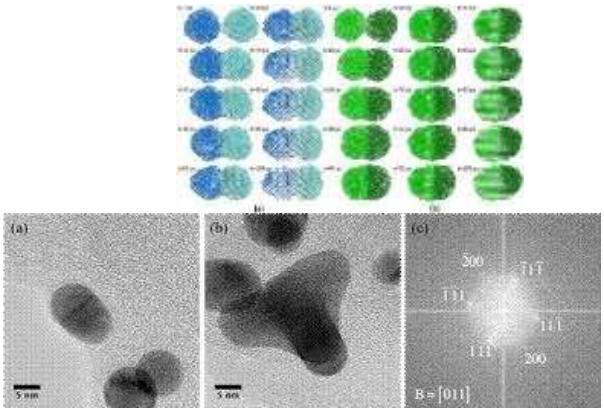

Twinned hemisphere structured nanoparticle

6. Applications of Metallic Nanoparticles:

Nanoparticles are used, or being evaluated for use, in many fields. The list below introduces several of the uses under development.

6.1 Nanoparticles in Medicine

(a) Researchers have confirmed that cerium oxide nanoparticles act as an antioxidant to remove oxygen free radicals that are present in a patient's bloodstream following a traumatic injury. The nanoparticles absorb the oxygen free radicals and then release the oxygen in a less dangerous state, freeing up the nanoparticle to absorb more free radicals.

(b) The nanoparticles protect the vaccine, allowing the vaccine time to trigger a stronger immune response.

(c) Nanodiamonds with protein molecules attached can be used to increase bone growth around dental or joint implants.

(d) Chemotherapy drugs attached to nanodiamonds is used to treat brain tumors. Chemotherapy drugs attached to nanodiamonds is also used to treat leukemia.

6.2 Nanoparticles in Manufacturing and Materials

(a) A synthetic skin that may be used in prosthetics has been established with both self remedial capability and the ability to sense pressure. The material is a composite of nickel nanoparticles and a polymer. If the material is held together after a cut it seals together in about 30 minutes giving it a self healing ability.

(b) Silicate nanoparticles can be used to provide a barrier to glass (for example oxygen), moisture in a plastic film used for packaging. This could slow down the process of spoiling or out in food.

(c) Zinc oxide nanoparticles can be dispersed in industrial coatings to protect wood, plastic and textiles from exposure of UV rays.

(d) Silicon dioxide crystalline nanoparticles can be used to fill gaps between carbon fibres, thereby strengthening tennis racquets.

(e) Silver nanoparticles in fabric are used to kill bacteria, making clothing odor-resistant.

6.3 Nanoparticle in Environment

(a) Researchers are using photo catalytic copper tungsten oxide nanoparticles to break down oil into biodegradable compounds. The nanoparticles are in a grid that provides high surface area for the reaction is activated by sunlight and can work in water, making them useful for cleaning up oil spills.

(b) Researchers are using gold nanoparticles embedded in a porous manganese oxide as a room temperature catalyst to breakdown volatile organic pollutants in air.

(c) Iron nanoparticles are being used to clean up carbon tetrachloride pollution in ground water.

(d) Iron oxide nanoparticles are being used to clean arsenic from water wells.

6.4 Nanoparticle in Energy and Electronics

(a) Researchers have used nanoparticles called nanotetrapods studded with nanoparticles of carbon to develop low cost electrodes for fuel cells. This electrode may be able to replace the expensive platinum needed for fuel cell catalysts.

(b) Researchers at Georgia Tech, the University of Tokyo and Microsoft Research have developed a method to print prototype circuit boards

using standard inkjet printers. Silver nanoparticle ink was used to form the conductive lines needed in circuit boards.

(c) Combining gold nanoparticles with organic molecules creates a transistor known as a NOMFET (Nanoparticle Organic Memory Field-Effect Transistor). This transistor is unusual in that it can function in a way similar to synapses in the nervous system.

(d) A catalyst using platinum-cobalt nanoparticles is being developed for fuel cells that produce twelve times more catalytic activity than pure platinum. In order to achieve this performance, researchers anneal nanoparticles to form them into a crystalline lattice, reducing the spacing between platinum atoms on the surface and increasing their reactivity.

(e) Researchers have demonstrated that sunlight, concentrated on nanoparticles, can produce steam with high energy efficiency. The "solar steam device" is intended to be used in areas of developing countries without electricity for applications such as purifying water or disinfecting dental instruments.

(f) A guide free solders reliable enough for space missions and other high stress environments using copper nanoparticles.

(g) Silicon nanoparticles coating anodes of lithium-ion batteries can increase battery power and reduce recharge time.

(h) Semiconductor nanoparticles are being applied in a low temperature printing process that enables the manufacture of low cost solar cells.

(i) A layer of closely spaced palladium nanoparticles is being used in a hydrogen sensor. When hydrogen is absorbed, the palladium nanoparticles swell, causing shorts between nanoparticles. These shorts lower the resistance of the palladium layer.

(j) photoswitchable short-chain dyads [19-22] and their nanocomposites (when nanoparticles combine with a short-chain dyad) possess great applications in molecular electronics, designing of molecular components of photovoltaic cells and artificial light energy converters, energy storage devices etc.

6.5 Nanoparticles in Paints

One of the most interesting aspects of metal nanoparticles is that their optical properties depend strongly upon the particle size and shape. Bulk Au looks yellowish in reflected light, but thin Au films look blue in transmission. This characteristic blue color steadily changes to orange, through several tones of purple and red, as the particle size is reduced down to ~3 nm. The nanoparticles attracted attention as color materials and the possibility of their use has been examined in various fields. Spraying with the clear colored coating containing the nanoparticles increased the depth of the red background even more, and since the car is in the shade there is almost no diffuse reflection. The red color becomes a feature of paints containing nanoparticles. Paints that contain nanoparticles cannot be removed as easily as can classical paint. However, because of high costs, paints with nanoparticles are used only in limited applications. Metal nanoparticles have also been used in enamel color paints in pottery. Conventional enamel color has used paints with mixed transition metals in the pulverization (glass frit) of glass. If, instead of transition metal paints, Au nanoparticles were used, then high quality red paint could be made with high transparency. Research into iron oxide nanoparticles in paints has also been carried out.

6.6 Nanoparticles in Micro-wiring

Metal nanoparticle paste is used for circuit pattern formation of a printed wired board in the electronic industry. The melting point of metal nanoparticles decreases relative to bulk metals, so that circuit formation impossible on polymer base material is attainable using a conventional electric conduction paste. Further-more, whenever particles at the nanoscale are used, the wiring width is thin to a nano level. Formation of nanoparticle wiring can use an ink-jet method, a method that is both inexpensive and requires shorter times than vacuum evaporation and photolithographic methods that are typically used. Generally, Au is used to make the metal nanoparticle paste. However, it is expensive, so that substitution of Cu nanoparticles has been proposed. Cu nanoparticles tend to be oxidized so that the process requires the presence of anti-oxidants.

6.7 Nanoparticles in Medical Treatments

Just as the surface plasmon resonance is seen in a metal nanoparticle, an increase in the quantity of nanoparticles raises the scattering intensity. Taking advantage of this feature, the application to specific molecule recognition in a living body tissue is expected. For example, by covering the cancer cell surface it becomes possible to distinguish a healthy cell from a cancer cell by the presence of antibodies joined to the Au nanoparticle. Although the Au nanoparticle junction with the antibody is nicely distributed in the healthy cell, when a cancer cell exists the antibodies are concentrated mostly at the Au nanoparticle. The imaging at various wavelengths is performed by a change in the shape of the nanoparticle. Moreover, if a protein and a functional molecule were joined to the Au nanoparticle, it could also be used for imaging cells other than

cancer cells. In this way the nanoparticles are widely used in the field of medical treatment.

7. Conclusion

In this review article the author has been involving himself to explain the details information regarding the formation of metal nanoparticles. Through this one can make an idea about metal nanoparticles. The physical properties of surface plasmon resonance (SPR) has been reported here. Various size of nanoparticles and its properties has been explained elaborately. The shape of nanoparticles is an important factor that determines the nature of the surface plasmon resonance has been described in this review article. The structural properties of the nanoparticles and their utility in the world of nano science has been explored. The details applications of nanoparticles in various fields are the key features of this review article.

References

1. Hadis Daraee , Ali Eatemadi , Elham Abbasi , Sedigheh Fekri Aval , Mohammad Kouhi, Abolfazl Akbarzadeh; Artif Cells Nanomed Biotechnol; (2016), **44(1),** 410-22.
2. Suriya Rehman, Abuzar Ali et al; in Modeling and Control of Drug Delivery Systems; (2021)
3. Satoshi Horikoshi and Nick Serpone; Microwaves in Nanoparticle Synthesis, First Edition Edited by Satoshi Horikoshi and Nick Serpone; 2013 Wiley-VCH Verlag GmbH & Co. KGaA. Published 2013 by Wiley-VCH Verlag GmbH & Co. KGaA.
4. L. A. Dykman, S. A. Staroverov, V. A. Bogatyrev & S. Yu. Shchyogolev; Nanotechnologies; (2010), **5,** 748–761

5. Geert Van der Snickt, Olivier Schalm, Joost M. A. Caen; Manfred Schreiner; January Studies in Conservation; (2006) **51(3),** 212-222

6. Rajpal Singh , Thathan Premkumar, Ji-Young Shin, Kurt E. Geckeler; Carbon Nanotube and Gold-Based Materials: A Symbiosis First published; (2010); https://doi.org/10.1002/chem.200901609

7. Michael Faraday's recognition of Ruby Gold: The birth of modern nanotechnology (2007), Gold Bulletin **40(4),** 267-269, DOI: 10.1007/ BF03215598

8. Edy Wijaya, Cédric Lenaerts, Sophie Maricot, Sabine Szunerits; Current Opinion in Solid State and Materials Science; (2011), **15(5)**, 208-224, DOI: 10.1016/j.cossms.2011.05.001

9. Faten Bashar Kamal Eddin, Yap Wing Fen; Molecules; (2020), ***25*(12),** 2769; https://doi.org/10.3390/molecules25122769

10. Yeonsu Lee, Jiwon Kim, Sungmin Sim, Ignacio Llamas-Garro, Jungmu Kim; Micromachines; (2021), **12(8),** 998; https://doi.org/10.3390/mi12080998

11. Advait Chhatre, Praveen Solasa, Suvarna Sakle, Rochish Thaokar, Anurag Me hra; Colloids and Surfaces A: Physicochemical and Engineering Aspects; (2012), **404,** 83-92

12. Eudenilson L. Albuquerque, Michael G. Cottam; Polaritons in Periodic and Quasiperiodic Structures; (2004)

13. Kenshin Takemura; Biosensors (Basel); (2021), **11(8),** 250; doi: 10.3390/ bios11080250

14. Kentaro Tomita, Yiming Pan, Atsushi Sunahara, Kouichiro Kouge, Hakaru Mizoguchi, Katsunobu Nishihara; Scientific Reports; (2023), **13,** Article number: 1825

15. Surface Plasmon Resonance Spectroscopy of Gold NanoparticleCoated Substrates Use as an Indicator of Exposure to Chemical Warfare Simulants D. B. Pedersen & E. J. S. Duncan; (2005)

16. Erika C. Vreeland, John Watt, Gretchen B. Schober, Bradley G. Hance, Mariah J. Austin, Andrew D. Price, Benjamin D. Fellows, Todd C. Monson, Nicholas S. Hudak, Lorena Maldonado-Camargo, Ana C. Bohorquez, Carlos Rinaldi, Dale L. Huber; Chem. Mater.; (2015), **27,** 17, 6059–6066; https://doi.org/10.1021/acs.chemmater.5b02510

17. Chao Chen, Ross A. L. Wylie, Daniel Klinger, Luke A. Connal; Chem. Mater.; (2017), **29,** 5, 1918–1945; https://doi.org/10.1021/acs.chemmater.6b04700

18. Quan Zhang, Kohei Kusada, Dongshuang Wu, Tomokazu Yamamoto, Takaaki Toriyama, Syo Matsumura, Shogo Kawaguchi, Yoshiki Kubota, Hiroshi Kitagawa; J. Am. Chem. Soc.; (2022), **144,** 9, 4224–4232; https://doi.org/10.1021/jacs.2c00583

19. I. Mitra, S. Paul, M. Bardhan, S. Das, M. Saha, A. Saha, T. Ganguly; Chem. Phys. Letters. (2019), **726,** 1-6.

20. G. D. Pal, S. Paul, M. Bardhan, A. De, T. Ganguly; Spectrochim.Acta Part A: Molecular and Biomolecular Spectroscopy (2017), **180,** 168-174

21. P. Chakraborty, S. Yadav, A. De, M. Bardhan, P. Kumbhakar, S. Biswas, H. Sankar De Sarkar, T. Ganguly ; J. Nanosci. Nanotechnol. (2016), **16,** 7411-7419

22. S. Fukuzumi, K. Ohkubo, H. Imahori, J. Shao, Z. Ou, G. Zheng, Y. Chen, R.K. Pandey, M. Fujitsuka, O. Ito, K.M. Kadish; J. Am. Chem. Soc. (2001), **123,** 10676-10683.

INDIAN JOURNAL OF THEORETICAL PHYSICS, VOL 70, NOS. 3 & 4, 2022

One Day Seminar by CITP in Collaboration with Physics Department of RKM Residential College Narendrapur, Kolkata

One day Seminar on " Recent Trends of Physics and Mathematics" to celebrate 70^{th} Anniversary of Calcutta Institute of Theoretical Physics was held jointly by CITP and Physics Department of Ramkrishna Mission Residential College, Narendrapur on 8^{th} December , 2022. The following Memorial lectures were presented in the seminar.

 # 1.Prof. S. Ghosh Memorial Lecture on " Sum of Two Squares"

Speaker: **Prof. Shashi Mohan Srivastava**, Visiting Professor of Mathematics, IACS, Jadavpur, Kolkata

 # 2.Prof. S. D. Chatterjee Memorial Lecture on " Quantum Statistics"

Speaker: **Prof. Jayanta Kumar Bhattacharjee**, Emeritus Professor of Physics, IACS, Jadavpur, Kolkata

Both the lectures were highly interactive. About 80 UG students and teachers from different Colleges of Kolkata participated in the Seminar and asked relevant and interesting questions to understand the subjects. The Speakers encouraged the advanced learners to study the subjects in details so that they can acquire in depth knowledge. The seminar ended with vote of thanks by Dr. Malay Purkait, Associate Professor and Head of the Department of Physics, RKM Residential College, Narendrapur, Kolkata.

INFORMATION TO AUTHORS

Manuscripts should represent results of original works on theoretical physics or experimental physics with theoretical background or on applied mathematics. Letters to the Editor and Review articles in emerging areas are also published. Submission of the manuscript will be deemed to imply that it has not been published previously and is not under consideration for publication elsewhere (either partly or wholly) and further that, if accepted, it will not be published elsewhere. It is the right of the Editorial Board to accept or to reject the paper after taking into consideration the opinions of the references.

Manuscripts may be submitted in pdf/MS word format to **admin@citphy.org or susil_vcsarkar@yahoo.co.in** Online submission of the paper through our **website: www.citphy.org** is also accepted. The file should be prepared with 2.5 cm margin on all sides and a line spacing of 1.5.

The title of the paper should be short and self-explanatory. All the papers must have an abstract of not more than 200 words, the abstract page must not be a part of the main file. Abstract should be self-contained. It should be clear, concise and informative giving the scope of the research and significant results reported in the paper. Below the abstract four to six key words must be provided for indexing and information retrieval.

The main file should be divided into sections (and sub-sections, if necessary) starting preferably with introduction and ending with conclusion. Displayed formula must be clearly typed (with symbols defined) each on a separate line and well-separated from the adjacent text. Equations should be numbered with on the right-hand side consecutively throughout the text. Figures and Tables with captions should be numbered in Arabic numerals in the order of occurrence in the text and these should be embedded at appropriate places in the text. Associated symbols must invariably follow SI practice.

References should be cited in the text by the Arabic numerals as superscript. All the references to the published papers should be numbered serially by Arabic numerals and given at the end of the paper. Each reference should include the author's name, title, abbreviated name of the journal, volume number, year of publication, page numbers as in the simple citation given below :

For Periodicals : Sen, N. R. - On decay of energy spectrum of Isotopic Turbulence, 1. Appl. Phys. **28,** No. 10, 109-110 (1999).

1. Mikhilin, S. G. - Integral Equations, Pergamon Press, New York (1964).
2. Hinze, A. K. - Turbulence Study of Distributed Turbulent Boundary Layer Flow, Ph. D, Thesis, Rorke University (1970).

The corresponding author will receive page proof, typically as a pdf file. The proof should be checked carefully and returned to the editorial office within two or three days. Corrections to the proof should be restricted to printing errors and made according to standard practice. At this stage any modifications (if any) made in the text should be highlighted.

To support the cost of publication of the journal, the authors (or their Institutions) are requested to pay publication charge ₹ 200/- per printed page for authors of Indian Institutes and US$ 20 for others. Publication charges to be sent directly to **CALCUTTA INSTITUTE OF THEORETICAL PHYSICS, 'BIGNAN KUTIR', 4/1 MOHAN BAGAN LANE, KOLKATA-700004, INDIA.**

A pdf of the final publisher's version of the paper will be sent to the corresponding author.

All communications are to be sent to the Secretary, Calcutta Institute of Theoretical Physics, 'BignanKutir', 4/1, Mohan Bagan Lane, Kolkata-700004, India. E-mail:susil_vcsarkar@yahoo.co.in

For details please visit our website www.citphy.org

Indian Journal of Theoretical Physics

Vol-70

JANUARY, 2022 – JUNE, 2022

C O N T E N T S

1. Density Functional Theory in Two-Dimensional Quantum Materials
   – *M. Bora and P. Deb* 7
2. Fiber Optics Communication
   – *Asit K. Datta* 39

JULY, 2022 – DECEMBER, 2022

C O N T E N T S

1. The Kinetic Energy Spectrum for Turbulence in a Stably Stratified Fluid : Kolmogorov or The Elusive Bolgiano-Obukhoy?
   – *Jayanta K Bhattacharjee* 85
2. On MHD Blood Flow Through Permeable Bifurcated Arteries in Tumor Treatments.
   – *Anup Kumar Karak and Ruma Bagchi* 113
3. A Brief Review on Metallic Nanoparticles
   – *Subhendu Chandra* 129
4. One Day Seminar by CITP in Collaboration with Physics Department of RKM Residential College, Narendrapur, Kolkata 149

PUBLICATIONS
OF
CALCUTTA INSTITUTE OF THEORETICAL PHYSICS
"BIGNAN KUTIR"
4/1, Mohan Bagan Lane, Kolkata-700 004, India
Phone : +91-33-25555726

INDIAN JOURNAL OF THEORETICAL PHYSICS (ISSN : 0019-5693)
Research Journal containing Original Papers, Review Articles and Letters to the Editor is published quarterly in March, June, September and December and circulated all over the world.

Subscription Rates
₹ 1500 per volume (for Bonafide Indian Party)
US$ 350 (for Foreign Party)

Back Volume Rates
₹ 1500 per volume (for Bonafide Indian Party)
US$ 350 per volume or Equivalent Pounds per volume

Books Written by Prof. K. C. Kar, D. Sc.

- **INTRODUCTION TO THEORETICAL PHYSICS [Vol. I and Vol. II (Acoustics)]** Useful to students of higher physics
  Price :₹ 60 or US $ 10 per volume
- **WAVE STATISTICS : Its principles and Applications**
  Useful to Post Graduate and Research students
  Price :₹ 80 or US $ 12
- **STATISTICAL MECHANICS : PRINCIPLES AND APPLICATIONS [Vol. I and Vol. II]** Useful to Advanced students of theoretical Physics
  Price :₹ 120 or US $ 15
- **A NEW APPROACH TO THE THEORY OF RELATIVITY**
  Useful to Post Graduate and advanced students
  Price :₹ 50 or US $ 8

Order may be sent directly to Calcutta Institute of Theoretical Physics
"BignanKutir", 4/1, Mohan Bagan Lane, Kolkata-700 004, India